

Children's Mercy Kansas City

SHARE @ Children's Mercy

Manuscripts, Articles, Book Chapters and Other Papers

1-1-2012

EAE/ASE recommendations for image acquisition and display using three-dimensional echocardiography.

Roberto M. Lang

Luigi P. Badano

Wendy Tsang

David H. Adams

Eustachio Agricola

See next page for additional authors

Let us know how access to this publication benefits you

Follow this and additional works at: <https://scholarlyexchange.childrensmercy.org/papers>



Part of the [Cardiology Commons](#), [Cardiovascular Diseases Commons](#), [Cardiovascular System Commons](#), and the [Investigative Techniques Commons](#)

Recommended Citation

Lang, R. M., Badano, L. P., Tsang, W., Adams, D. H., Agricola, E., Buck, T., Faletra, F. F., Franke, A., Hung, J., de Isla, L., Kamp, O., Kasprzak, J. D., Lancellotti, P., Marwick, T. H., McCulloch, M. L., Monaghan, M. J., Nihoyannopoulos, P., Pandian, N. G., Pellikka, P. A., Pepi, M., Roberson, D. A., Shernan, S. K., Shirali, G. S., Sugeng, L., Ten Cate, F. J., Vannan, M. A., Zamorano, J. L., Zoghbi, W. A., . . . EAE/ASE recommendations for image acquisition and display using three-dimensional echocardiography. *Eur Heart J Cardiovasc Imaging* 13, 1-46 (2012).

This Article is brought to you for free and open access by SHARE @ Children's Mercy. It has been accepted for inclusion in Manuscripts, Articles, Book Chapters and Other Papers by an authorized administrator of SHARE @ Children's Mercy. For more information, please contact hlsteel@cmh.edu.

Creator(s)

Roberto M. Lang, Luigi P. Badano, Wendy Tsang, David H. Adams, Eustachio Agricola, Thomas Buck, Francesco F. Faletra, Andreas Franke, Judy Hung, Leopoldo Pérez de Isla, Otto Kamp, Jaroslaw D. Kasprzak, Patrizio Lancellotti, Thomas H. Marwick, Marti L. McCulloch, Mark J. Monaghan, Petros Nihoyannopoulos, Natesa G. Pandian, Patricia A. Pellikka, Mauro Pepi, David A. Roberson, Stanton K. Shernan, Girish S. Shirali, Lissa Sugeng, Folkert J. Ten Cate, Mani A. Vannan, Jose Luis Zamorano, William A. Zoghbi, American Society of Echocardiography, and European Association of Echocardiography

EAE/ASE Recommendations for Image Acquisition and Display Using Three-Dimensional Echocardiography

Roberto M. Lang, MD, FASE*[‡], Luigi P. Badano, MD, FESC^{†‡}, Wendy Tsang, MD*, David H. Adams, MD*, Eustachio Agricola, MD[†], Thomas Buck, MD, FESC[†], Francesco F. Faletra, MD[†], Andreas Franke, MD, FESC[†], Judy Hung, MD, FASE*, Leopoldo Pérez de Isla, MD, PhD, FESC[†], Otto Kamp, MD, PhD, FESC[†], Jaroslaw D. Kasprzak, MD, FESC[†], Patrizio Lancellotti, MD, PhD, FESC[†], Thomas H. Marwick, MBBS, PhD*, Marti L. McCulloch, RDCS, FASE*, Mark J. Monaghan, PhD, FESC[†], Petros Nihoyannopoulos, MD, FESC[†], Natesa G. Pandian, MD*, Patricia A. Pellikka, MD, FASE*, Mauro Pepi, MD, FESC[†], David A. Roberson, MD, FASE*, Stanton K. Sherman, MD, FASE*, Girish S. Shirali, MBBS, FASE*, Lissa Sugeng, MD*, Folkert J. Ten Cate, MD[†], Mani A. Vannan, MBBS, FASE*, Jose Luis Zamorano, MD, FESC, FASE[†], and William A. Zoghbi, MD, FASE*

From the University of Chicago, Chicago, Illinois (R.M.L., W.T.); University of Padua, Padua, Italy (L.P.B.); Mount Sinai Medical Center, New York, New York (D.H.A.); San Raffaele Hospital, Milan, Italy (E.A.); University Duisburg-Essen, Essen, Germany (T.B.); Fondazione Cardiocentro Ticino, Lugano, Switzerland (F.F.F.); Klinikum Region Hannover-Siloah, Hannover, Germany (A.F.); Massachusetts General Hospital, Boston, Massachusetts (J.H.); University Clinic San Carlos, Madrid, Spain (L.P.I., J.L.Z.); VU University Medical Center, Amsterdam, The Netherlands (O.K.); Medical University of Lodz, Lodz, Poland (J.D.K.); University of Liege, Liege, Belgium (P.L.); Cleveland Clinic, Cleveland, Ohio (T.H.M.); Methodist DeBakey Heart and Vascular Center, The Methodist Hospital, Houston, Texas (M.L.M., W.A.Z.); King's College Hospital, London, United Kingdom (M.J.M.); Imperial College, London, United Kingdom (P.N.); Tufts University Medical Center, Boston, Massachusetts (N.G.P.); Mayo Clinic, Rochester, Minnesota (P.A.P.); Centro Cardiologico Monzino, IRCCS, Milan, Italy (M.P.); The Heart Institute for Children, Oak Lawn, Illinois (D.A.R.); Harvard Medical School, Boston, Massachusetts (S.K.S.); Medical University of South Carolina, Charleston, South Carolina (G.S.S.); Yale University, New Haven, Connecticut (L.S.); Erasmus MC, Rotterdam, The Netherlands (F.J.T.C.); and ASE Writing Group, Morrisville, North Carolina (M.A.V.).

Keywords

Echocardiography • Two-dimensional • Three-dimensional • Transthoracic • Transesophageal

Reprint requests: American Society of Echocardiography, 2100 Gateway Centre Boulevard, Suite 310, Morrisville, NC 27560 (E-mail: ase@asecho.org).

*Writing Committee of the American Society of Echocardiography.

[‡]Drs. Lang and Badano contributed equally to this report.

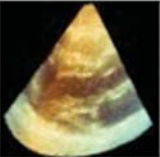
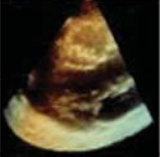


[†]Writing Committee of the European Association of Echocardiography.

The following authors reported no actual or potential conflicts of interest in relation to this document: Eustachio Agricola, MD, Thomas Buck, MD, Judy Hung, MD, FASE, Leopoldo Pérez de Isla, MD, PhD, FESC, Otto Kamp, MD, PhD, Patrizio Lancellotti, MD, PhD, FESC, Thomas H. Marwick, MBBS, PhD, Marti L. McCulloch, MBA, RDCS, FASE, Petros Nihoyannopoulos, MD, FESC, Mauro Pepi, MD, FESC, Wendy Tsang, MD, Jose Luis Zamorano, MD, FESC, FASE, and William A. Zoghbi, MD, FASE. The following authors reported relationships with one or more commercial interests: Roberto M. Lang, MD, FASE, lectured for Philips Ultrasound; Luigi P. Badano, MD, FESC, has received software and equipment from GE Healthcare and TomTec for research and testing purposes and is on the speakers' bureau of GE Healthcare; David H. Adams, MD, serves as a consultant and inventor with royalties for Edwards Lifesciences; Andreas Franke, MD, FESC, received software and hardware support for research purposes from Philips, GE Healthcare, and Siemens; Jaroslaw D. Kasprzak, MD, FESC, has served as a speaker for GE Healthcare, Philips, and Siemens; Mark J. Monaghan, PhD, FESC, has served as a speaker and received research support from Philips, GE Healthcare, Siemens, and TomTec; Natesa G. Pandian, MD, has received equipment support and served as a speaker for Philips, Toshiba, and GE Healthcare; Stanton K. Sherman, MD, FASE, served as a speaker for Philips Healthcare; Girish S. Shirali, MBBS, FASE, served as a consultant, advisory board member, recipient of research grants, and lecturer for Philips Medical Systems; Folkert J. Ten Cate, MD, was a three-dimensional course director for a Philips teaching course; and Mani A. Vannan, MBBS, FASE, served on the speakers' bureau and received research support and honoraria from Lantheus and Siemens.

Attention ASE: Members: ASE has gone green! Visit www.aseuniversity.org to earn free continuing medical education credit through an online activity related to this article. Certificates are available for immediate access upon successful completion of the activity. Nonmembers will need to join ASE to access this great member benefit!

Published on behalf of the European Society of Cardiology. All rights reserved. © The Authors 2012. For permissions please email: journals.permissions@oup.com

Table 1 Methods to avoid gating artifacts and improve 3D data set quality

Problem	Image	Recommended Suggestions for Correction
Over Gain		<ul style="list-style-type: none"> • Reduce power gain to mid range – no greater than 60 • Reduce compression/dynamic range in mid range • Optimize gain setting with TGC's (slightly over gain) • Background depth should be noted
Under Gain		<ul style="list-style-type: none"> • Increase overall gain with TGC's (slightly over gain) • Compression/Dynamic range in mid range • Increase power Gain in mid range – between 50 and 60 • Background depth should be noted
Stitch Artifact		<ul style="list-style-type: none"> • Rhythm Artifact – wait for semi consistent rate • Respiratory Artifact – have patient take a deep breath in, note optimal image quality and have the patient hold • Use reference plane only for cropping and analysis to minimize artifact appearance or use real time
Poor Resolution		<ul style="list-style-type: none"> • Compromise between volume rate and spatial resolution • Increase line density (will drop volume rate) • Interrogate area of interest in orthogonal planes rather than transverse • Optimize frequency, compression, focus and maps.

TGC, Time gain control.

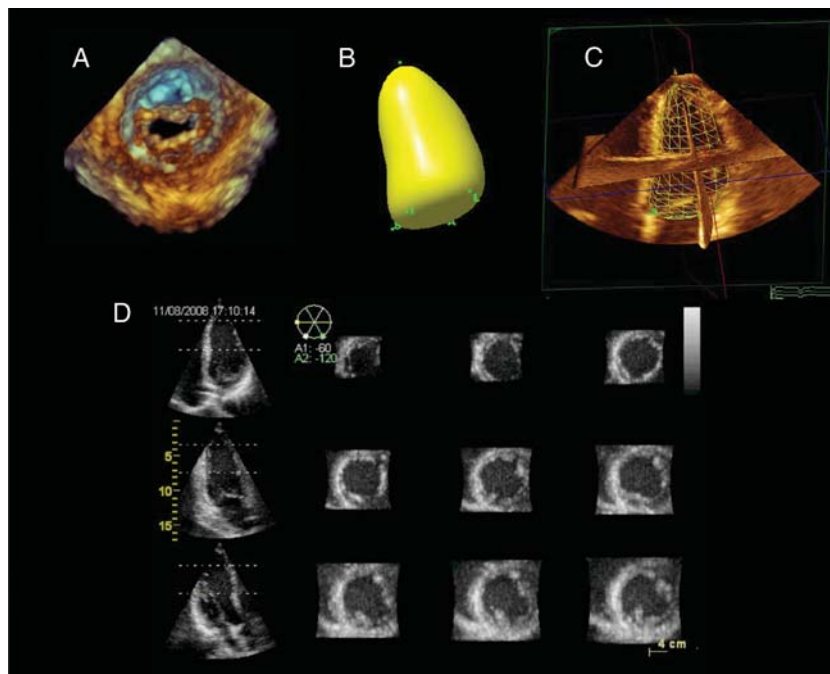


Figure 4 Three-dimensional echocardiographic data sets can be viewed interactively using different 3D visualization and rendering software packages. The techniques used to display 3D images can be divided into four broad categories: volume rendering (A), surface rendering (B), wireframe (C), and 2D tomographic slicing (D).

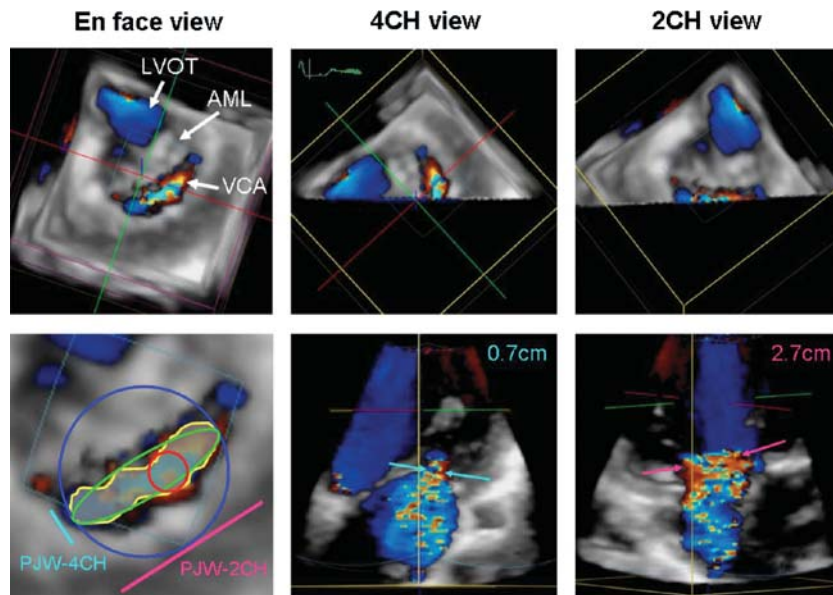


Figure 5 Transthoracic 3DE color Doppler images of a functional mitral regurgitation jet. En face view of the asymmetric vena contracta as seen from the left ventricle (*top left*). Note that the vena contracta is located along the commissural line. Quantitative assessment of the vena contracta using the en face plane (*bottom left*). The data set was cropped to create four-chamber (4CH) and two-chamber (2CH) views of the vena contracta, which can be shown en face view (*top middle and top right*) and perpendicular by tilting 90° upward (*bottom middle and bottom right*), demonstrating the eccentricity of the vena contracta. AML, Anterior mitral valve leaflet; LVOT, LV outflow tract; PJW, proximal jet width; VCA, vena contracta area.

(if available) or use narrow-angled 3D acquisition mode. Last, select the highest resolution option that accommodates the volume of interest.

A complete 3D TTE exam requires multiple acquisitions from the parasternal, apical, subcostal, and suprasternal transducer positions. Table 2 lists the 2D TTE views from which 3DE data sets should be acquired. Because the volume-rendered 3D data set can be cropped to display a variety of intracardiac structures by choosing different cut planes as an alternative to “view” (referred to heart’s orientation to the body axis), “anatomic planes” (referred to the heart itself) can be used to describe image orientation.¹⁴ The most frequently used cropping planes are (1) the *transverse plane*, a horizontal plane that runs perpendicular to the long axis of the body dividing the heart into superior and inferior segments; (2) the *sagittal plane*, a vertical plane that divides the heart into right and left segments; and (3) the *coronal plane*, a vertical plane that divides the heart into anterior and posterior segments (Figure 8).

8. Transesophageal 3DE Examination Protocol

A comprehensive 3DE examination using the matrix TEE transducer usually starts with real-time imaging modes such as live and narrow-angled acquisition.¹⁵ However, the gated 3DE modes, including 3D color flow Doppler, should also be used whenever ECG and respiration gating requirements are permissible, to take advantage of the improved spatial and temporal

resolution of these wide-angled acquisitions. Three-dimensional TEE data sets acquired using a matrix array include both the area and depth of the imaging plane, thereby requiring less probe manipulation for data acquisition compared with a standard 2D TEE examination. Furthermore, unique en face 3DE views with infinite real-time rotational and cropping plane capabilities, as well as offline quantitative analyses, should result in accurate diagnoses and ultimately improved clinical decision making.^{14,16–724} Although a systematic approach to performing a comprehensive 3D TEE examination is recommended, it is recognized that not all views may be optimally obtained in all patients and that additional unconventional views may be required to obtain additional detailed information in patients with complex pathologies.

Initially, a real-time 3DE and a subsequent gated 3DE data set should be obtained from the midesophageal views to determine the overall function of the left and right ventricles and to identify structural valve abnormalities. Table 3 describes the recommended views to obtain 3D images of cardiac structures using transesophageal echocardiography. Table 4 demonstrates how to display 3D TEE images of the cardiac valves from the original 2D TEE views. Offline analyses of the gated 3DE data set acquired from the midesophageal five-chamber view can be performed to obtain quantitative measures of LV global and regional function.

9. Assessment of the LV

Accurate and reproducible quantitative assessment of LV size and function are pivotal for diagnosis, treatment, and prediction of

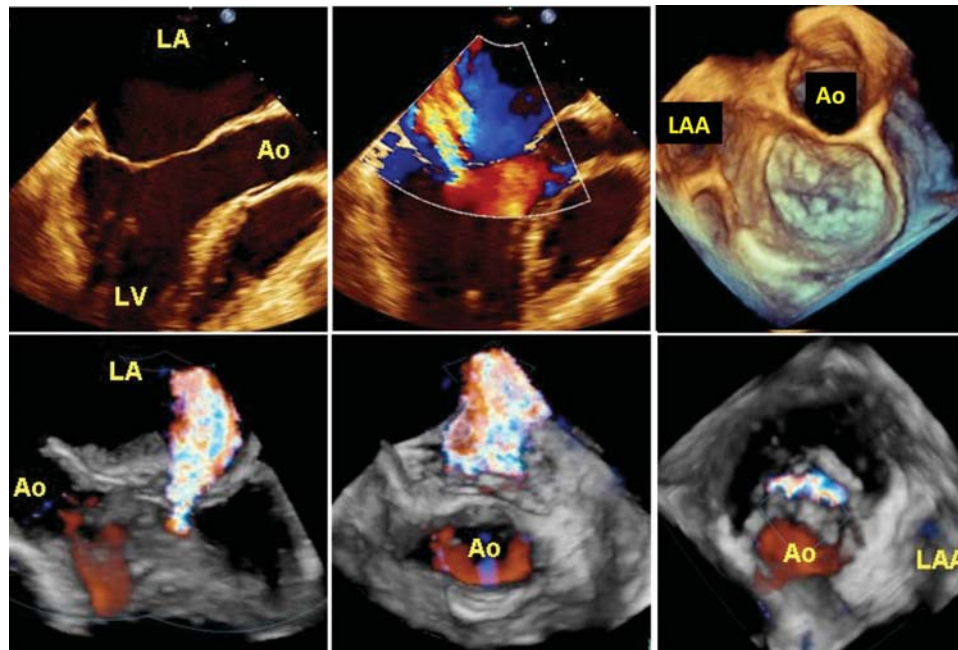


Figure 6 Example of 3D assessment of functional mitral regurgitation by 3D transesophageal echocardiography and 3D color Doppler. Two-dimensional cross-sectional views demonstrating mitral leaflet tethering and tenting (*top left*) causing significant eccentric mitral regurgitation (*top middle*). Three-dimensional echocardiographic view to the mitral valve shows only moderate focal nodular degeneration of mitral leaflet (*top right*). Cropping of a 3D color Doppler data set reveals a vena contracta area, which is narrow in the five-chamber view (*bottom left*), broad in the two-chamber view (*bottom middle*), and asymmetric along the commissural line in an en face view to the mitral valve (*bottom right*). Ao, Aorta; LA, left atrium; LAA, left atrial appendage; LV, left ventricle.

prognosis of structural heart diseases. In this regard, the most important contribution of 3D echocardiography may be in LV quantification.²⁵ Cumbersome acquisition methods and lack of user-friendly analysis software initially precluded widespread use of 3D echocardiography, but the advent of matrix transducers, together with impressive improvements in semiautomated volumetric analysis, has allowed 3D echocardiography to evolve from a complicated and time-consuming research tool into a simple and fast imaging modality ready for everyday clinical use.

a. Anatomy and Limitations of 2DE Assessment

The purpose of 3D imaging of the left ventricle is to provide volume and ejection fraction measurements independent of geometric assumptions regarding LV shape.²⁵ The landmarks used for this process are the mitral annulus and LV apex, which are used to initiate edge detection by semiautomated quantification software. Other anatomic features of importance are the LV trabeculae and papillary muscles, which should be included within the LV cavity for the calculation of LV volumes. The trabeculae are small structures that are often poorly visualized with 3DE imaging, and the use of LV opacification with contrast is the best way to ensure that they are incorporated within the LV cavity.^{26–29}

The assessment of wall motion requires a frame of reference to allocate segments. The 17-segment model distinguishes six

segments (inferoseptal, anterosseptal, anterior, lateral, inferolateral, inferior) in the base and mid left ventricle, four segments (septal, anterior, lateral, inferior) in the apex, and the apical cap.³⁰ This segmentation is based on the mitral annulus, papillary muscles, and apical portion of the LV cavity to define the planes in the longitudinal dimension. In the transverse dimension, the segments comprise 60° arcs, starting at the midpoint of the septum, which itself is defined by the anterior and posterior RV insertion points of the septum. A little more problematic is the definition of regional LV volume, currently defined in most programs by the space between the endocardial border and a centerline through the LV cavity. This virtual landmark may shift with alterations of LV mass and remodeling after myocardial infarction, leading to underestimation of serial regional volume changes. The use of an externally defined frame of reference could overcome this problem, but it is unclear how this can be readily achieved.

LV structural changes that can be identified with 3D echocardiography include ventricular septal defects and masses such as LV thrombi or tumors. The sites of these are usually described by reference to the relevant landmarks (mitral annulus, LV outflow tract, and apex) or segmentation.

Despite the utility and established role of 2D echocardiography to assess LV function, it has a number of important limitations for LV imaging, including foreshortening, malrotation, and angulation. Because of the geometric assumptions of 2D echocardiography, volumetric measurements may be inaccurate if the acquisition of

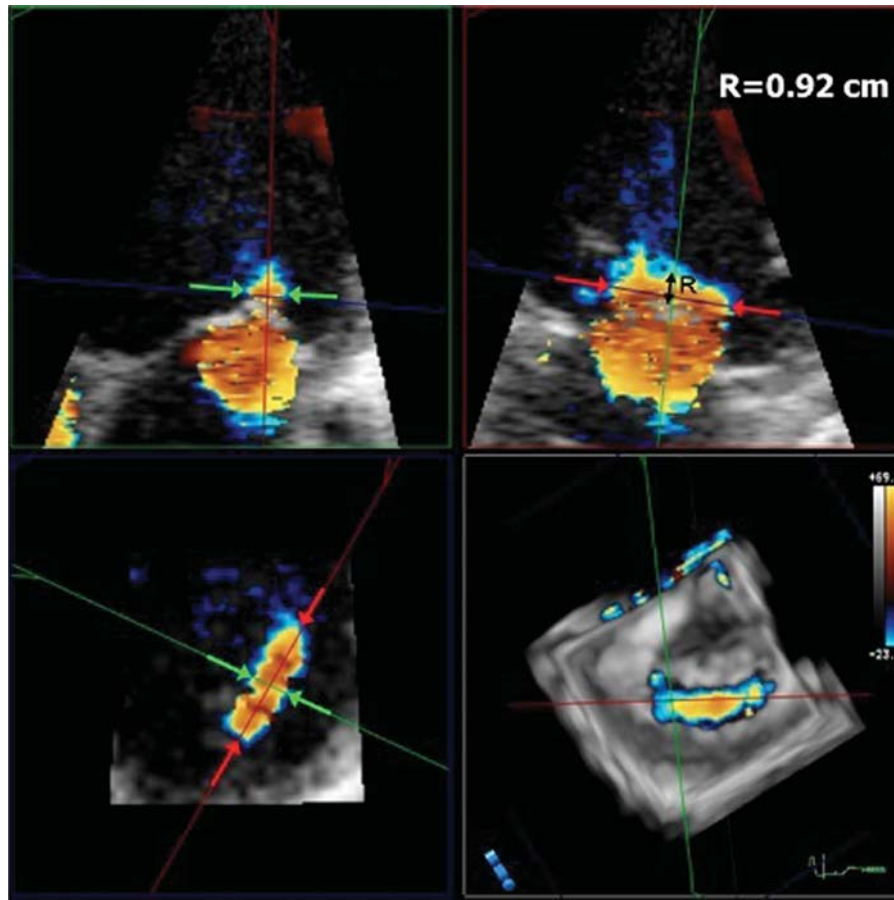


Figure 7 Measurement of vena contracta dimensions from a 3D TEE color Doppler data set (*bottom right*) using 3D analysis software. The data set is cropped to create a four-chamber (*top left*) and a two-chamber view (*top right*). Note that the vena contracta width is smaller when measured on the four-chamber view compared with the two-chamber view. The cropping plane can be adjusted to present an en face view of the vena contracta from which a planar area of 1.11 cm^2 (*bottom right*) can be measured. R, Proximal isovelocity surface area radius.

2D images is suboptimal. Likewise, appropriate interpretation of regional LV responses to stress requires all vascular territories to be imaged and for analogous segments to be displayed at rest and stress.

As with its use in other situations, there are fundamentally two approaches to the application of 3D echocardiography. The first involves the use of a full-volume data set to create standard 2D images in which the cut planes are optimized to ensure that they are “on axis”; this is the strategy used for segmental wall motion assessment and tracing of LV borders for volume calculations. In segmental imaging, there are benefits of obtaining orthogonal views to confirm wall motion abnormalities in any segment. The second is a display of rendered images that provides a 3D impression of a structure, such as might be used for the assessment of LV mass or thrombus.

These benefits are obtained at the cost of technical shortcomings of 3D echocardiography. The probe footprint of most 3D transthoracic transducers is large, which contributes to difficulty in imaging the anterior and lateral walls because of interference from ribs. Recently, newer 3D transthoracic transducers have

been developed with smaller footprints to overcome these limitations. Second, there is lower line density and therefore lower spatial resolution of 3D echocardiography, which may be partly readdressed with the use of LV opacification with contrast.²⁸ Third, 3D echocardiography has lower temporal resolution than 2D echocardiography because of the lower volume rate that is attainable with 3D echocardiography. This can be addressed by narrowing the 3D sector and stitching multiple subvolumes, but at the risk of creating stitching artifacts and with specific limitations in irregular rhythms or inability to hold the breath.

b. Data Acquisition and Cropping

Data Acquisition

A 3DE acquisition of the entire left ventricle generally takes <10 sec. Although all standard acquisition windows for echocardiography are available and useful for 3D acquisitions, the ideal and generally preferred approach for the acquisition of a full-volume LV data set is the apical one (Tables 2, 3, and 5). Depending on the shape of the heart and its position within the chest, a more

Table 2 Protocol for transthoracic 3D echocardiography

Protocol For Three-Dimensional Transthoracic Echocardiography

Aortic Valve	Left Ventricle/Right Ventricle	Pulmonic Valve
Parasternal long-axis view with and without color (narrow angle and zoomed acquisitions)	Apical four-chamber view (narrow and wide angle acquisition) Please note that the image must be tilted to place the right ventricle in the center of the image for right ventricular acquisition	Parasternal right ventricular outflow tract view with and without color (narrow angle and zoomed acquisitions)
Mitral Valve	Interatrial and Interventricular Septum	Tricuspid Valve
Parasternal long-axis view with and without color (narrow angle and zoomed acquisitions)	Apical four-chamber view (narrow angle and zoomed acquisitions)	Apical four-chamber view with and without color (narrow angle and zoomed acquisitions)
Apical four-chamber view with and without color (narrow angle and zoomed acquisitions)		Parasternal right ventricular inflow view with and without color (narrow angle and zoomed acquisitions)

off-axis position may be appropriate to ensure the acquisition of the entire left ventricle. To guarantee optimal image quality, transducer frequency and overall gain should be adjusted accordingly. The best sequence for image optimization is to follow the 2D images with real-time 3D images—although there is limited value in real-time imaging of the left ventricle (except for structural changes such as mass or thrombus), this step is of value to optimize gain settings—which should be typically higher than those used for 2D echocardiography. Acquisition of the full-volume data set can be guided by a split-screen display of orthogonal views, which can itself be used for simultaneous imaging in two or three planes. The full-volume acquisition should be made during a breath hold to minimize the risk for breathing (stitch) artifacts. As discussed above, contrast LV opacification is often of value.²⁶⁻²⁹

c. Orientation and Display

There is no general agreement on how the imaging planes should be displayed. The proposed “apex-down” 3D display has not been widely adapted for LV imaging, perhaps because LV imaging is “3D-guided 2D.” The preference of the writing group is to orient images so that right-sided structures are on the left-hand side and the apex is up (Figure 9).

d. Analysis Methods

Volume rendering is of primary value for demonstration of structural abnormalities. Within the left ventricle, these might include thrombi, masses and septal defects. This approach is of limited value for the quantification of LV function.

Surface rendering is of primary value for global and regional functional measurements, including 3D echocardiography-guided 2D imaging for measurement of LV volume, ejection fraction and mass. Most vendors offer software packages for both online and

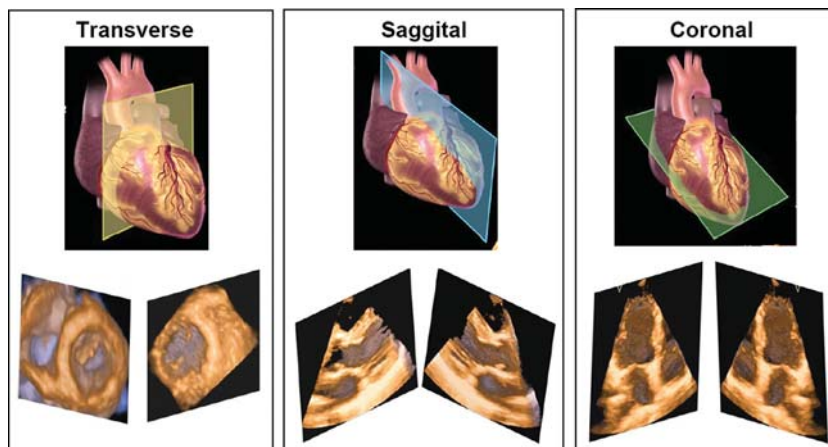


Figure 8 Cropping of the heart in the transverse plane, a horizontal plane that runs parallel to the ground dividing the heart into superior and inferior segments (*top left*); sagittal plane, a vertical plane that divides the heart into right and left segments (*center*); and coronal plane, a vertical plane that divides the heart into anterior and posterior segments (*top right*). The lower panels present the 3D views that result from these cut planes.

Table 3 Protocol for transesophageal 3D echocardiography

Protocol For Three-Dimensional Transesophageal Echocardiography		
Aortic Valve	Left Ventricle/Right Ventricle	Pulmonic Valve
60° mid-esophageal, short-axis view with and without color (zoomed or full-volume acquisition)	Left ventricle - 0° to 120° mid-esophageal views encompassing the entire ventricle (full-volume acquisition)	90° high-esophageal view with and without color (zoomed acquisition)
120° mid-esophageal, long-axis view with and without color (zoomed or full-volume acquisition)	Right ventricle - 0° to 120° mid-esophageal views with the right ventricle tilted to be in the center of the image (full-volume acquisition)	120° mid-esophageal, 3-chamber view with and without color (zoomed acquisition)
Mitral Valve 0° to 120° mid-esophageal views with and without color (zoomed acquisition)	Interatrial Septum 0° with the probe rotated to the interatrial septum (zoomed or full-volume acquisition)	Tricuspid Valve 0° to 30° mid-esophageal, 4-chamber view with and without color (zoomed acquisition) 40° transgastric view with anteflexion with or without color (zoomed acquisition)

offline quantitative analysis of the left ventricle. Typically, this process involves segmentation of the 3DE data set into several equiangular 2D longitudinal planes after initialization of a few anatomic landmarks, such as the mitral annulus and apex, in several conventional 2D planes. If necessary, manual corrections to the endocardial borders can be performed,³¹ after which a semiautomated blood endocardial interface detection algorithm allows the calculation of cavity contours and display of their changes during the cardiac cycle providing a volume-versus-time curve (Figure 10). A surface-rendered cavity cast of the left ventricle is then constructed, from which LV volume is computed without geometric assumptions, directly from voxel counts.

Wireframe models are effective for defining sections of the left ventricle in position and time. These 3DE data can be used to assess LV synchrony, regional strain, curvature, and wall stress. However, these steps are computationally intensive and are not performed in routine practice.

The analysis of regional function is more complex to communicate than global function or even shape. One option is a polar map

display incorporating wall motion scoring; a similar and more dynamic process may be illustrated using contraction front mapping (Figure 11), which illustrates the spatial distribution of contraction and relaxation.

e. Clinical Validation and Application

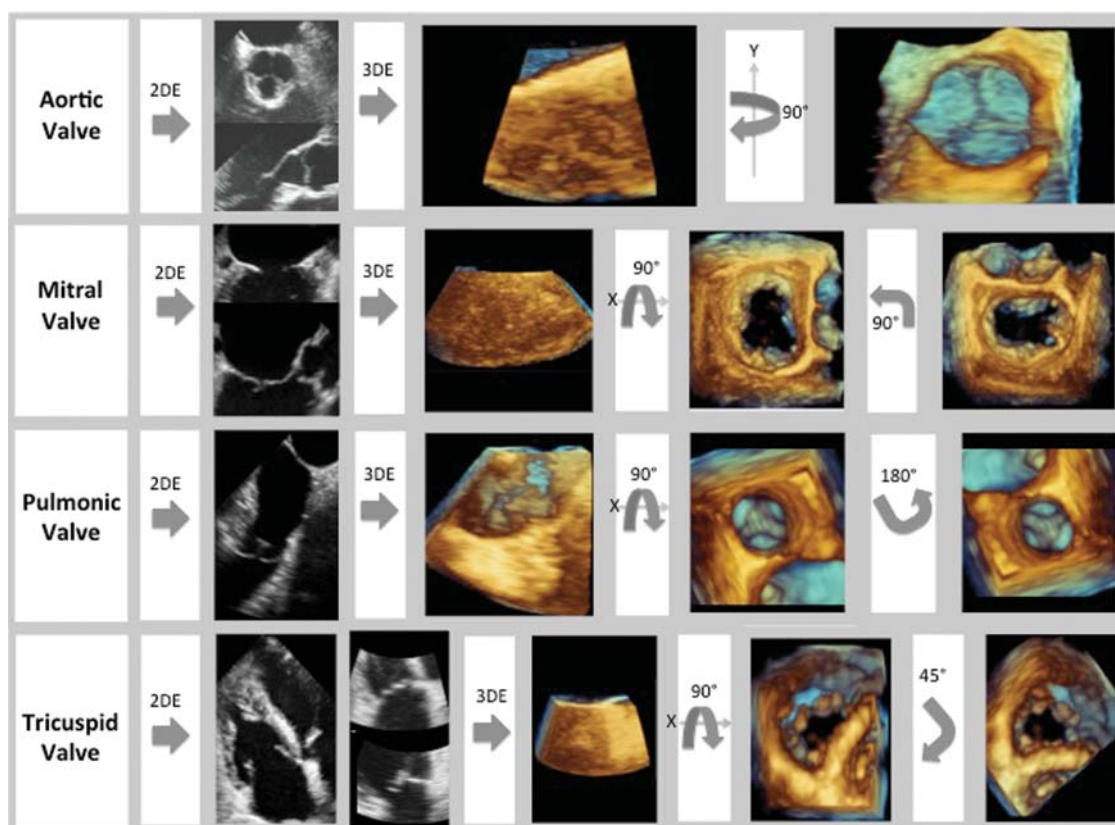
LV Structural Abnormalities (e.g., Thrombus, Ventricular Septal Defect)
These are assessed using visual assessment and 3DE color flow mapping.

Global LV Functional Measurements

These include volumes, ejection fraction, LV shape, and regional and global strain. Of these, LV volumes and ejection fraction are the closest to clinical application. This measurement of LV volume and function is rapid, more accurate and reproducible than with 2DE, and has an accuracy that is similar to magnetic resonance imaging, although the variability may be higher as a result of varying image quality and operator expertise.³² The availability of LV cavity shape allows the extraction of additional quantitative information in patients with LV dysfunction (e.g., the 3D sphericity index).³³ The assessment of 2D global strain is an interesting potential marker of global function; whether this measurement can be reliably assessed with 3D imaging remains undefined at present.

Despite the high correlation with magnetic resonance imaging as the reference technique, several studies using both manual and semiautomated contour detection have shown significant underestimation of 3D echocardiography-derived LV volumes.^{28,31,34–49} The potential reasons for the underestimation are numerous, but systematic underestimation of LV volumes by 3D echocardiography compared with magnetic resonance imaging may be largely explained because 3D echocardiography, unlike magnetic resonance imaging, cannot consistently differentiate between the myocardium and the trabeculae.³² To minimize intertechnique differences, tracing the endocardium to exclude trabeculae in the LV cavity is recommended for 3D echocardiography. As well, one-beat acquisitions may not successfully capture true end-systole, because of the reduced temporal resolution. This will lead to inaccurate end-systolic volume calculations and ejection fraction measurements.

The reproducibility of LV volume and function measurements by 3D echocardiography has been assessed in multiple studies.^{31,35,50,51} Most of these studies were part of larger studies in which series of patients were analyzed twice by one observer and by a second observer. Less variation is reported than with 2D echocardiography. The best reproducibility was obtained in studies that selected patients on the basis of good image quality.⁵² Differences between observers are less likely to be of technical origin. Although some differences have been found to be statistically significant between different baseline settings with different semiautomated endocardial contour tracing algorithms, they do not seem clinically relevant. The normal values of LV end-diastolic and end-systolic volume have not been established by gender and body size and so are not provided in this document.

Table 4 Acquisition and presentation of cardiac valves

Aortic valve (top row): First, with 2D transesophageal echocardiography, the aortic valve should be centered in the acquisition boxes in two orthogonal views. One view should be of the aortic valve in the midesophageal 60° short-axis view and the second in the 120° long-axis view. Then, live 3D mode should be used to optimize gain settings. Subsequently, full-volume acquisition should be performed. If the 3D volume is acquired from the previously described 2D views, to display the aortic valve, it must be rotated clockwise, 90° around the y axis, so that the aortic valve is presented as seen from the ascending aorta with the right coronary cusp located at the 6 o'clock position. **Mitral valve (second row):** First, with 2D transesophageal echocardiography, the mitral valve should be centered in the acquisition boxes in two different views. One view should be of the mitral valve in the midesophageal 90° "two-chamber" view and the other in the 120° long-axis view. From those views, the full-volume acquisition should be performed. Once acquired, the volume should be rotated counterclockwise, 90° around the x axis. This presents the mitral valve as viewed from the left atrium. Finally, the mitral valve should be rotated counterclockwise in plane so that the aortic valve is located at the 12 o'clock position. **Pulmonic valve (third row):** First, with 2D transesophageal echocardiography, the pulmonic valve should be centered in the acquisition box in the 0° high-esophageal view. From this view, the full-volume acquisition should be performed. Once it is acquired, the image volume should be rotated around the x axis, counterclockwise 90°. This will display the pulmonic valve en face as if viewed from the pulmonary artery. Finally, to display the pulmonic valve properly, the image must be rotated in plane 180° so that the anterior leaflet is located at the 12 o'clock position. **TV (bottom row):** First, with 2D transthoracic echocardiography, the TV should be acquired from an off-axis apical four-chamber view. The acquisition boxes should be centered on the TV in two orthogonal views. From these views, the full-volume acquisition should be performed. After acquisition, the image volume should be rotated around the x axis, counterclockwise 90°. This will present the TV as if viewed from the right atrium. Then, the valve should be rotated in plane 45° so that the septal leaflet is located at the 6 o'clock position.

LV Mass

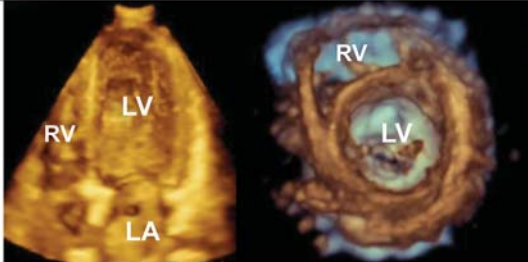
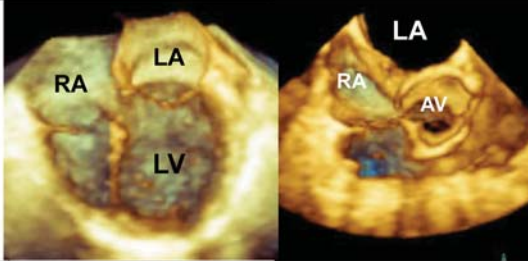
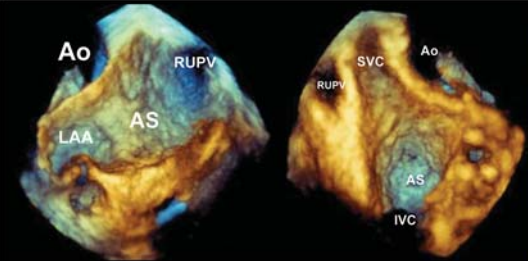
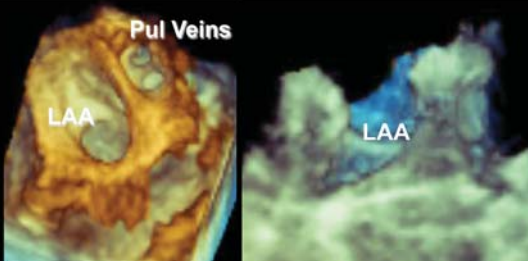
More user interaction is required to identify the epicardium for the calculation of LV mass. Despite a slight overestimation of LV mass by 3D echocardiography in comparison with magnetic resonance imaging measurements, the accuracy of 3D echocardiography is similar to that of magnetic resonance imaging in most patients.^{35,42,53-57} However, there are wide limits of agreement, reflecting a number of issues. First, the use of innermost versus outermost endocardial contour tracing might explain measurement differences, as LV mass measurement increases with the inclusion of trabeculae into the LV wall. Second, LV mass measurement also relies on accurate visualization and tracing of the epicardial contour, which is even more challenging than endocardial tracing. Takeuchi et al.⁵⁸ and Pouleur et al.⁴⁸ used

echocardiographic analysis software that semiautomatically detected the endocardial surface and then calculated LV mass by arbitrarily adding 8.8 mm of wall thickness to the endocardial surface. Third, analysis of short-axis magnetic resonance images and long-axis 3DE images is distinctly different.

LV Dyssynchrony

For the analysis of LV dyssynchrony, individual LV segmental volumes are plotted versus time throughout the cardiac cycle. These plots allow measurement of temporal differences in segmental time to minimum volume. Regional minimal volume (i.e., maximal contraction) normally occurs at the same time in ventricular systole for all segments. In a left ventricle with dyssynchrony, there is dispersion in the timing of regional segments

Table 5 3DE presentation of cardiac structures

<p>Left Ventricle</p> <p>Display the left ventricle from in either the short axis view (left) or the apical four-chamber view (right).</p> <p>LA=left atrium, LV=left ventricle, RV=right ventricle</p>	
<p>Right Ventricle</p> <p>Display the right ventricle in the a four-chamber view (left) or the short-axis view (right) with the left atrium at the twelve o'clock position.</p> <p>AV=aortic valve, LA=left atrium, LV=left ventricle, RA=right atrium</p>	
<p>Interatrial Septum</p> <p>When viewed from the left atrium (left), the atrial septum should be oriented with the right upper pulmonary vein at the one o'clock position. When displayed as viewed from the right atrium (right), the superior vena cava should be located at the 11 o'clock position.</p> <p>AS=atrial septum, Ao=aorta, LAA=left atrial appendage, RUPV=right upper pulmonary vein, SVC=superior vena cava</p>	
<p>Left Atrial Appendage</p> <p>The left atrial appendage should be presented en-face from the left atrial perspective (left) with the pulmonary veins located superiorly or longitudinally (right).</p> <p>LAA=left atrial appendage, Pul Veins=pulmonary veins</p>	

reaching minimal volume as the diseased segments achieve minimal volume later in systole (Figures 10 and 11). The systolic dyssynchrony index (SDI) is calculated as the standard deviation of regional ejection times (time to regional minimal volume). Parametric images using color schemes representing timing differences in segmental contraction can be displayed in a “bull’s-eye” format, which is a practical tool for identifying and localizing areas of dyssynchrony.

The literature on 3DE dyssynchrony has focused on three major areas: (1) description of reference values and reproducibility of SDI in normal subjects and different patient subsets, (2) comparison of

3DE measurements of SDI with those using conventional methods (i.e., tissue Doppler), and (3) prediction of responses to cardiac resynchronization therapy (CRT) using 3D echocardiography–derived LV SDI.

Doppler tissue imaging has high temporal resolution but only provides information on longitudinal systolic myocardial contraction of the mid and basal segments, frequently with low reproducibility.⁵⁹ In contrast, 3D echocardiography evaluates all LV segments simultaneously. Three-dimensional echocardiography–derived LV SDI was described as highly predictive of response to CRT at 48 hours,⁶⁰ 6 months,^{61,62} and 1 year of follow-up.⁶³

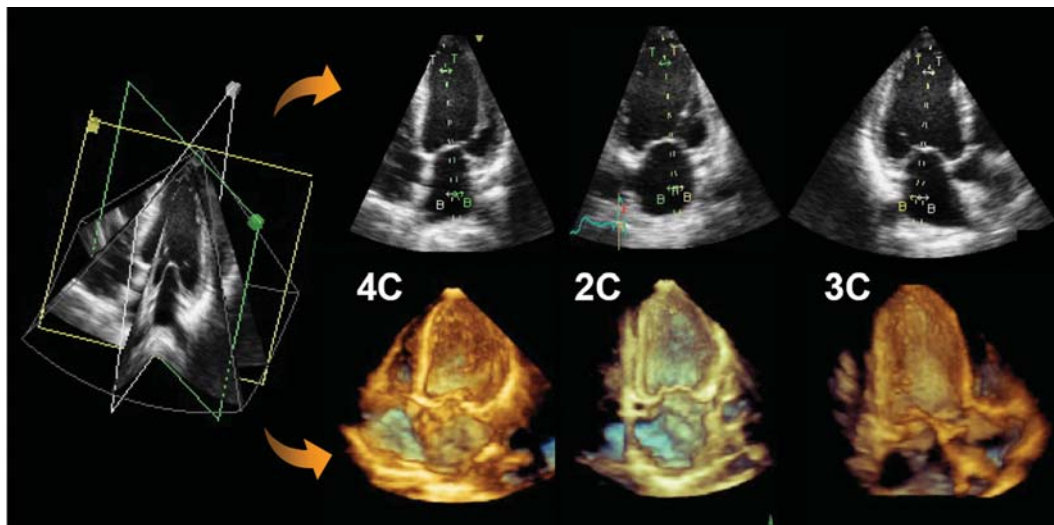


Figure 9 Example of a triplane 2DE acquisition. This mode is typically acquired from a single transthoracic apical echocardiographic window. A default setting of 60° increments between the three planes allows the simultaneous acquisitions of the four-chamber (4C) and two-chamber (2C) views as well as the apical long axis (*top*). Three-dimensional full-volume data sets cropped to provide 3DE views from the equivalent apical four-chamber and two-chamber views and long-axis views (*bottom*). 3C, Three-chamber.

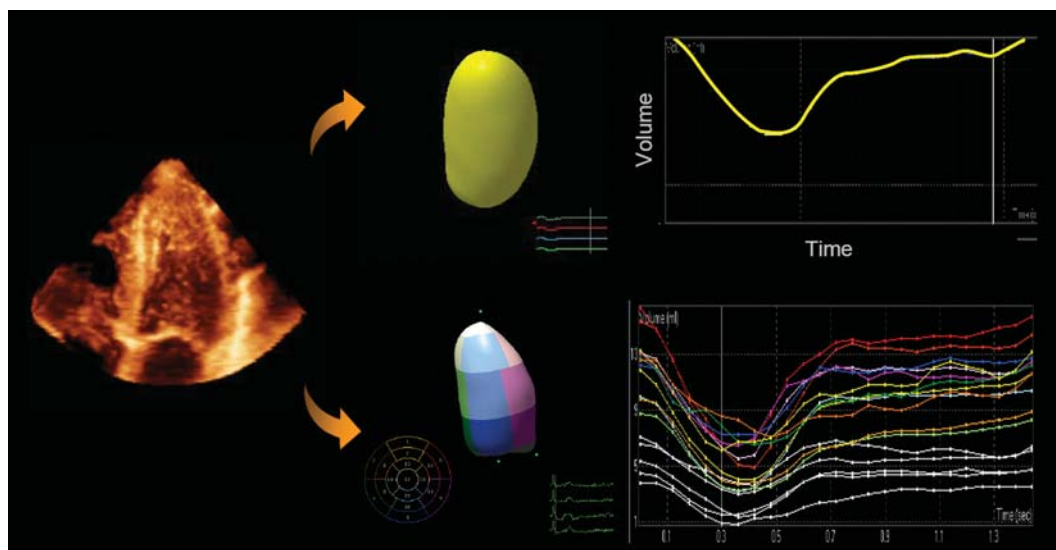


Figure 10 From a transthoracic 3DE data set of the left ventricle (*left*), the LV endocardium can be traced (*middle, top*) to obtain the LV volume throughout the cardiac cycle (*right, top*). As well, the LV endocardium can be divided according to the 17-segment model (*middle, top*), and the time each segment requires to attain minimal volume in the cardiac cycle can be identified (*right, bottom*).

Benefits from CRT have been defined as a $\geq 15\%$ reduction in LV end-systolic volume at follow-up,^{60,62,63} which can also readily be measured using 3D echocardiography.

Finally, the importance of optimal LV pacing lead position was emphasized in a 3DE study in which the responses to CRT were compared between patients with the LV pacing lead positioned at the site of maximal mechanical delay and those in whom the pacing lead was positioned distal to that site. LV function,

reverse remodeling, and peak oxygen consumption were significantly improved in patients with optimal LV pacing lead position guided by 3D echocardiography, whereas the opposite occurred with increasing distance between the optimal and the actual pacing site.⁶⁴ Currently, because these data come from small, single-center, nonrandomized studies, patients should not be selected for CRT on the basis of 3DE parameters until more data become available.

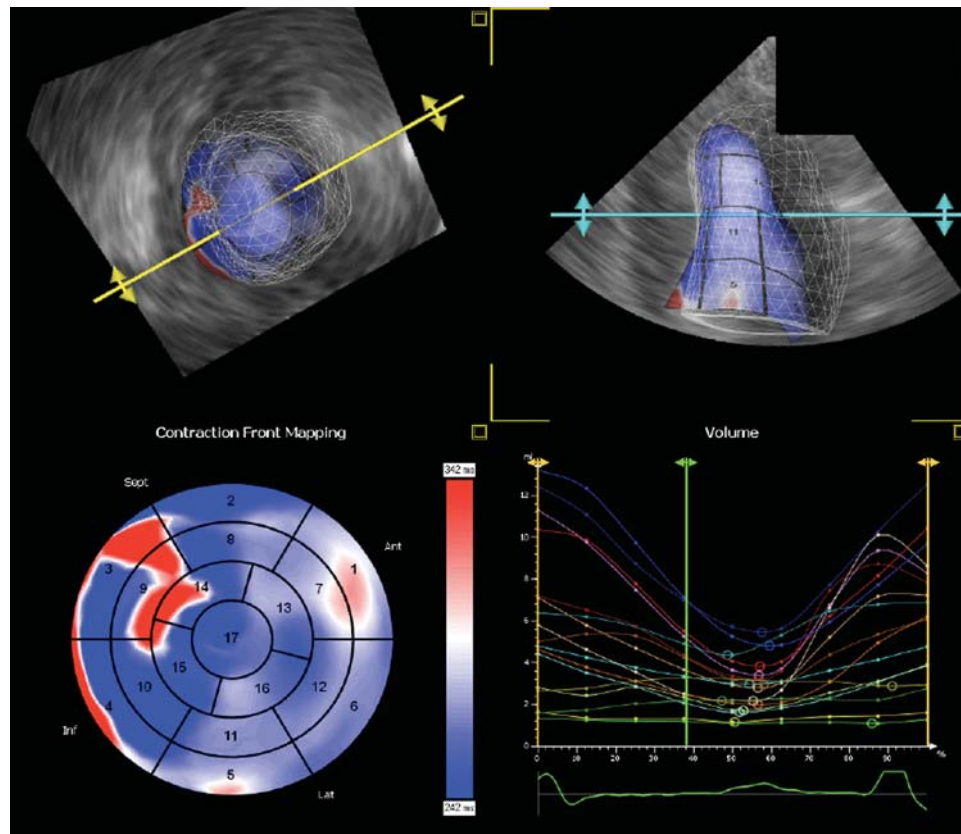


Figure 11 Three-dimensional TTE data set of the left ventricle as viewed from the apex (*left, top*) or anteriorly (*right, top*), with dynamic tracking of the LV endocardium. The end-diastolic LV endocardium is visualized as a mesh shell and the end-systolic endocardium as a solid shell. Seventeen-segment, bull's-eye map of contraction front mapping demonstrating the time required for each segment to reach minimal LV volume (*left, bottom*). Graph, with time along the x axis and volume along the y axis, demonstrating the time for each segment to reach minimal volume (*right, bottom*). Ant, Anterior; Inf, inferior; Lat, lateral; Sept, septum.

f. Future Perspectives

A large amount of evidence suggests that in the presence of adequate image quality, LV volumes and functional measurements by 3D echocardiography have closer limits of agreement with cardiac magnetic resonance measurements and better reproducibility than 2D echocardiography, making it the modality of choice for the everyday clinical evaluation of LV volumes and ejection fraction.⁶⁵ Furthermore, LV dyssynchrony assessment by 3D echocardiography might play a valuable role in the selection of patients for CRT through the prediction of response but also prove to be useful for the optimization of LV lead placement.⁶⁶ Other developments, such as 3D strain measurement⁶⁷ and LV shape analysis,³³ show great potential to become future clinical applications. Future advancements in hardware will facilitate the acquisition of wider angle pyramidal data with higher spatial and temporal resolution in a single cardiac cycle. To continue to enhance the clinical applicability of 3DE imaging, further improvements in automatic quantitative analysis software that will enable fast online measurements that are accurate and reproducible are required.

Currently, 3D TTE and TEE assessment of LV volumes and ejection fraction is recommended over the use of 2D

echocardiography, as it has been clearly demonstrated to provide more accurate and reproducible measurements.

10. Assessment of the RV

a. Anatomy and Limitations of 2DE Assessment

The right ventricle is composed of three anatomic and functional subunits, which extend from (1) the tricuspid valve (TV) annulus to the proximal os infundibulum, (2) the RV body to the apex, and (3) the RV outflow tract to the pulmonary valve. This divides the RV cavity into three sections: inlet, apical trabecular, and outlet, respectively. The musculature of the right ventricle extends from the atrioventricular to the ventriculoarterial junctions. The right ventricle is highly trabeculated, with several muscle bands, including the septoparietal trabeculations and the moderator band. From a functional point of view and because of the orientation of the RV fibers, global assessment of the right ventricle is difficult, with the two main sections contracting

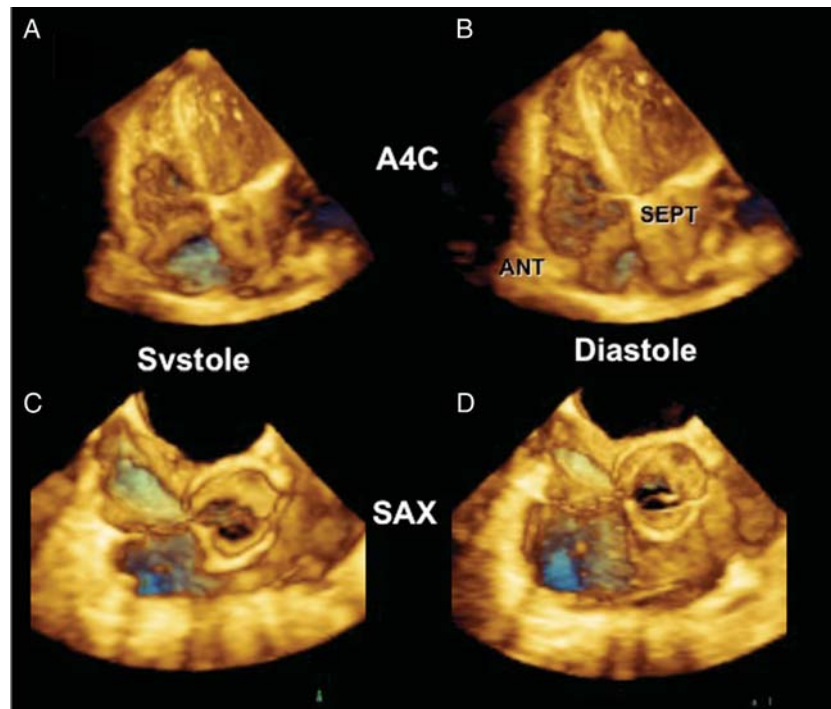


Figure 12 Three-dimensional TTE image of the right ventricle in systole (**A**) and diastole (**B**) as acquired from the apical four-chamber (A4C) window. Three-dimensional TTE image of the RV outflow tract in systole (**C**) and diastole (**D**) as acquired from the short-axis view (SAX) with the aortic valve in the center, the TV to the left, and the pulmonic valve to the right. ANT, anterior; SEPT, septum.

perpendicular to each other: the proximal (RV inflow) longitudinally and the distal (RV outflow) circumferentially.

Because of the peculiar RV morphology and function, 2D echocardiography has several limitations in the evaluation of the right ventricle, which can be readily overcome by a 3DE gated wide-angled acquisition, which enables complete assessment of its geometry, volumes, and ejection fraction (Figure 12 and 13), displaying the surfaces of the entire right ventricle including the inflow, apex, and outflow tracts.^{68,69}

b. Data Acquisition

Several methods and software packages have been used to evaluate the right ventricle. Three-dimensional data are acquired in a full-volume data set from the four-chamber apical view adapted to include the entire right ventricle (Tables 2 and 3). Three-dimensional echocardiographic data sets are typically digitally stored and then postprocessed offline. On-cart dedicated RV analysis software packages will be soon available, further facilitating the use of these measurements in clinical practice. Current RV analysis software displays 2D cut planes of the RV sagittal, four-chamber, and coronal views obtained from the full-volume 3DE data set.

c. Orientation and Display

The anatomy and pathology of the TV and the right ventricle are best visualized using volume-rendered images (Table 5). When performing volumetric analysis using semiautomated border tracking software data, the right ventricle may be displayed as a

wireframe or surface-rendered cast. Studies describing quantitative changes in tricuspid annular enlargement and leaflet tenting have used the wireframe method.⁷⁰ Cropping tools can be applied to 3DE data sets to visualize the RV inflow and outflow tracts. The TV can be displayed from both the right atrial and RV perspectives. The right atrial view of the TV should be modified to a surgeon's orientation, as seen in Figure 14. The TV should be displayed with the septal leaflet at the 6 o'clock position, irrespective of perspective. The right atrium and right ventricle can be visualized using multiple cut planes. A variety of axial cuts at the apex, mid, and base of the right ventricle can be obtained using the long axis of the left ventricle. In Figure 13, an axial cut plane of the right ventricle depicts a view of the TV and RV outflow tract on the left. Longitudinal cut planes can also demonstrate the right ventricle from a typical four-chamber view, coronal view, and RV inflow view. The position of these cut planes is represented on the axial view. The four-chamber view of the right ventricle demonstrates the RV free wall and septum. The coronal cut plane demonstrates the right atrium, TV (septal and posterior leaflets), RV inflow and outflow, and pulmonic valve. The RV inflow view shows the right atrium, anterior and posterior TV leaflets, and interventricular septum.

d. Analysis Methods

The current methods used to quantify RV geometry and functions include the method of disks, a rotational approach, and most recently a volumetric semiautomated border detection approach.

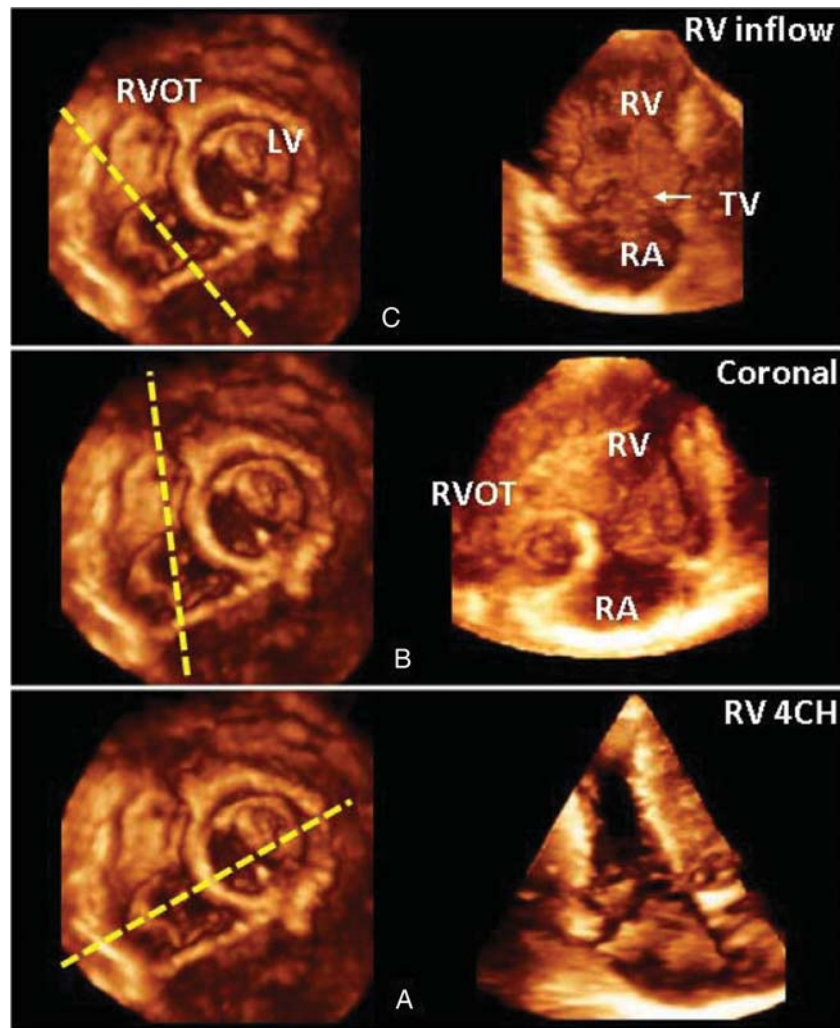


Figure 13 From a whole-heart transthoracic full-volume 3DE data set, a cropping plane can be used to obtain the following views of the right ventricle (RV): sagittal right ventricular inflow (*top left and right*), coronal (*middle left and right*), and four-chamber (4CH) view (*bottom left and right*). LV, Left ventricle; RA, right atrium; RVOT, right ventricular outflow tract.

Two of these methods are currently commercially available and are shown in Figure 15.

Method of Disks and Other Methods

A variety of options for offline 3DE reconstruction of the right ventricle exist. After acquisition and automatic display of the RV end-diastolic and end-systolic frames, the operator, in the axial plane, traces a contour of the endocardial border. These traced contours generate disks of fixed height (generally 10 mm) but of varying lengths and widths, as visualized in the other RV orthogonal views. The volume of the RV cavity is computed by adding the known areas of the axial traces obtained 10 mm apart (i.e., disk summation). The number of disks required to cover the entire right ventricle from base to apex varies from seven to eight depending on RV size.

Recently available software calculates RV volumes from end-diastolic and end-systolic endocardial border tracings of sagittal (to outline the TV in the best possible view), four-chamber (to

outline the apex), and coronal (to outline the RV outflow tract) 3D echocardiography–derived cross-sectional planes. The operator frequently needs to manually adjust the traced contours in each frame before reconstruction and quantitative analysis. Trabeculations are generally included in the endocardial rim, but the apical component of the moderator band is excluded from the cavity. The RV volumes are calculated by summation of the volumes for each slice through the complete data set. Each volume data set is imported into the application and manipulated by rotating, angulating, and slicing in any of the three displayed orthogonal planes. This software analysis, which uses a semiautomated border detection algorithm with manual correction options, was validated using in vitro models as well as in vivo using cardiac magnetic resonance as the gold standard.⁷¹

Volumetric Display

The different software packages create a surface-rendering cast of the right ventricle. The end-diastolic and end-systolic volumes as

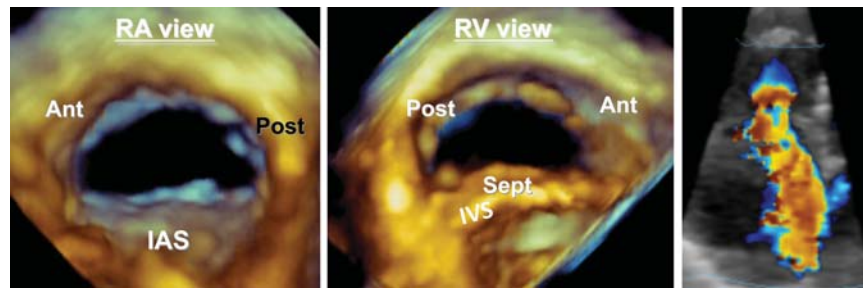


Figure 14 Three-dimensional TEE images of the TV, whether presented as viewed from the right atrium (left) or the right ventricle (middle), are oriented with the interatrial septum located inferiorly. Three-dimensional echocardiographic color Doppler image demonstrating flow convergence in tricuspid regurgitation (right). Ant, Anterior; IAS, interatrial septum; IVS, interventricular septum; Post, posterior; Sept, septum.

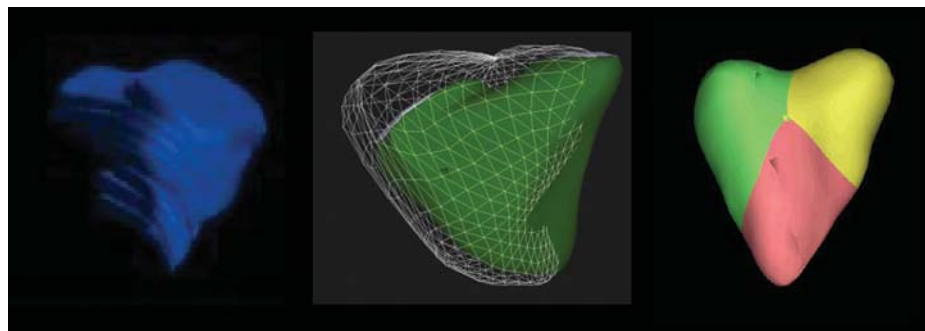


Figure 15 The RV volume can be determined from 3D echocardiographic data sets by the method of disks (left). Other methods include dynamic endocardial tracking with end-diastolic volumes presented by the mesh shell and end-systolic volumes presented by the solid shell (middle). The RV endocardial shell can be segmented for regional analysis (right).

well as RV ejection fraction are measured and automatically displayed. Segmental analysis of the three main sections of the right ventricle (inlet, apex, and outflow segments) may be performed. Curves of global and regional RV function may be generated and analyzed.

e. Clinical Validation and Application

Data on RV volumes and function are of diagnostic and prognostic importance in a variety of cardiac diseases, including valve disease, congenital heart disease, pulmonary hypertension, and heart failure. Three-dimensional echocardiography allows the quantification of volumes and function in normal subjects and patients,⁷² thereby allowing identification of patients with different degrees of severity of RV dilatation and dysfunction.⁷³ Several clinical studies have shown a good correlation between cardiac magnetic resonance and 3DE volumes and ejection fraction of the right ventricle in selected populations, with the majority of studies showing a slight underestimation of volumes compared with the reference technique.^{71,74–76} Differences in RV volumes have been demonstrated between men (129 ± 25 mL) and women (102 ± 33 mL), but adjusting to lean body mass (but not to body surface area or height) eliminated this difference.^{76–78} The use of 3D transthoracic

echocardiography has been validated^{79–81} in patients with pulmonary regurgitation, secundum atrial septal defects, tetralogy of Fallot repair, Ebstein's anomaly, and RV cardiomyopathy. The feasibility and utility of 3D transthoracic echocardiography for guidance of RV endomyocardial biopsies in children has also been demonstrated.⁸²

Assessment of RV function is of great interest in cardiovascular surgery, because right-sided heart failure is one of the most frequent causes of morbidity and mortality after valvular and congenital surgery, coronary artery bypass, and heart transplantation. This highlights the importance of an accurate preoperative assessment of the right ventricle to improve risk stratification and early and precise postoperative follow-up to optimize treatment. In this regard, 2DE and Doppler parameters (tricuspid annular plane systolic excursion, tissue Doppler imaging of the annulus) have several limitations, particularly in postoperative follow-up. The evaluation of RV volumes and ejection fraction using 3D echocardiography overcomes many of the limitations of 2DE methods.⁸³

Currently, 3DE assessment of RV volumes and ejection fraction shows great promise. However, routine clinical use is limited by the need for excellent quality transthoracic data sets for accurate analysis with software packages.

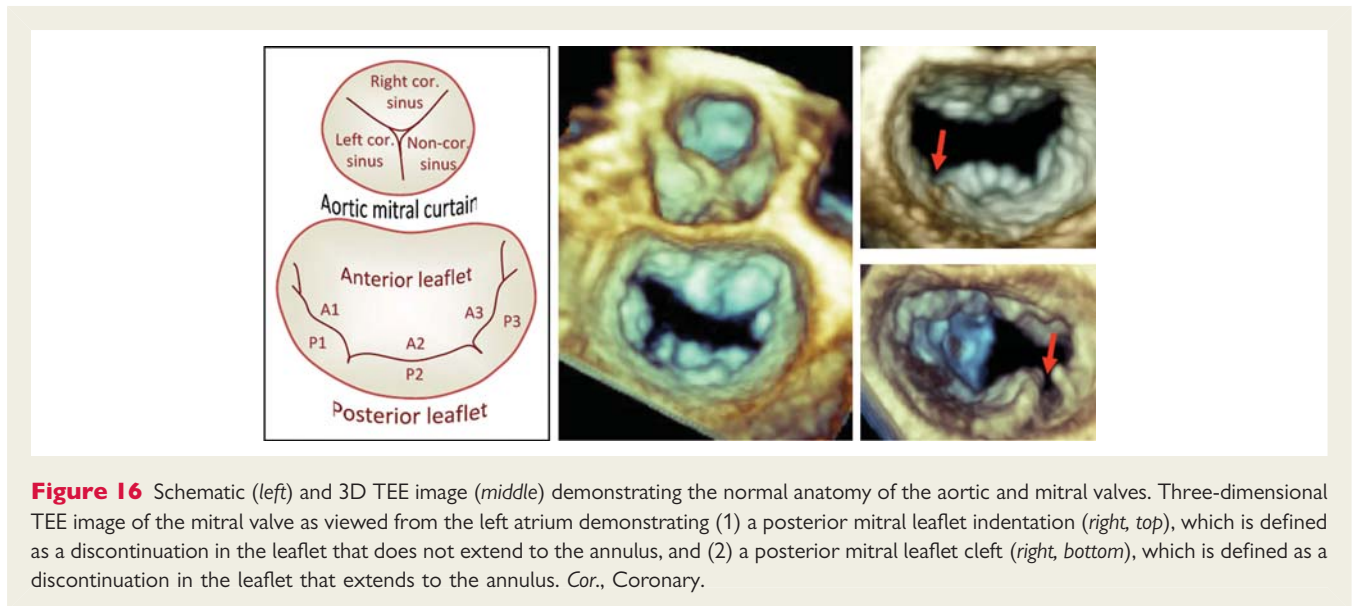


Figure 16 Schematic (left) and 3D TEE image (middle) demonstrating the normal anatomy of the aortic and mitral valves. Three-dimensional TEE image of the mitral valve as viewed from the left atrium demonstrating (1) a posterior mitral leaflet indentation (right, top), which is defined as a discontinuation in the leaflet that does not extend to the annulus, and (2) a posterior mitral leaflet cleft (right, bottom), which is defined as a discontinuation in the leaflet that extends to the annulus. Cor., Coronary.

11. Mitral Apparatus

a. Anatomy and Limitations of 2DE Assessment

The mitral apparatus is formed from the hyperbolic paraboloid (i.e., saddle) shaped annulus, the multiscalloped and indented leaflets connected by opposing anterolateral and posteromedial commissures, the subvalvular apparatus composed of a highly variable chordae tendineae arrangement with dual papillary muscles, and the LV wall attachments. Function of this apparatus requires an intricate coordination between multiple anatomic components, each of which has a unique functional geometry. Three-dimensional echocardiographic imaging modalities are ideal for interrogating the anatomy and function of each of the individual components of the mitral apparatus.⁸⁴

Mitral Leaflets

The anterior mitral valve leaflet has the larger radial surface and is attached to about one third of the annular circumference. The posterior leaflet has a larger circumferential attachment (two-thirds of the annulus) and is quadrangular in shape. Both leaflets are segmented into three individual scallops: A1, A2, and A3, the anterior, and P1, P2, P3, the posterior (from left to right, respectively; Figure 16). Leaflet segmentation is particularly useful to precisely localize prolapsing segments and anatomic lesions of the mitral valve. The coaptation line has an upward concavity and can be checked for visible leaks while in the closed position. The anterior mitral valve leaflet is in continuity with the left and noncoronary cusps of the aortic valve (aortic-mitral curtain⁸⁵), as seen from the LV perspective in a modified oblique view of the atrioventricular plane (Figure 16).

Three-dimensional TTE data set acquisitions for mitral valve visualization can be made either from the parasternal or the apical approach. A zoomed acquisition (allowing the highest temporal and spatial resolution) is best suited to detail mitral valve

leaflet anatomy and motion. A full-volume acquisition is required when the entire mitral valve apparatus needs to be assessed.

In contrast to conventional 2D echocardiography, which only displays the mitral valve leaflets en face from the LV perspective, 3D echocardiography enables en face visualization from both LV and left atrial perspectives. The latter view is also known as the “surgical view,” because it resembles the intraoperative image of the mitral valve after the surgeon, standing on the patient’s right side, opens the left atrium. Figure 16 displays the “surgical view” appearance of a normal mitral valve by 3D TEE volume rendering. In addition to the visualization of mitral valve leaflets (center) and left atrial appendage (left), this classic display enables visualization of the spatial relationship with the tricuspid annulus (right) and with the aortic valve (top, approximately at 1 o’clock) (Figures 16–18, Tables 4 and 6).

Overall, the posterior mitral valve leaflet is best visualized from the parasternal window, while the anterior leaflet can be well seen from both apical and parasternal windows.⁸⁶ The ventricular perspective of the mitral valve obtained from the apical window is the recommended approach for visualizing the anterior leaflet, while the prolapsing segments are appreciated from the surgical view of the valve, equally well from both parasternal and apical windows.⁸⁶ Beyond the en face view, 3D echocardiography allows practically any cut plane of an apical or parasternal data set to be used to obtain a conventional or unconventional display of the mitral valve leaflets. This may be necessary to precisely localize the abnormal mitral valve segment. Additionally, data obtained by 3D echocardiography have resulted in the recommendation that the diagnosis of mitral valve prolapse should not be made on the basis of the valve appearance in the 2DE four-chamber view.

Subvalvular Apparatus

The functional integrity of the subvalvular mitral apparatus can be appreciated from LV long-axis cut planes. En face views of the mitral valve from the LV perspective allow evaluation of the

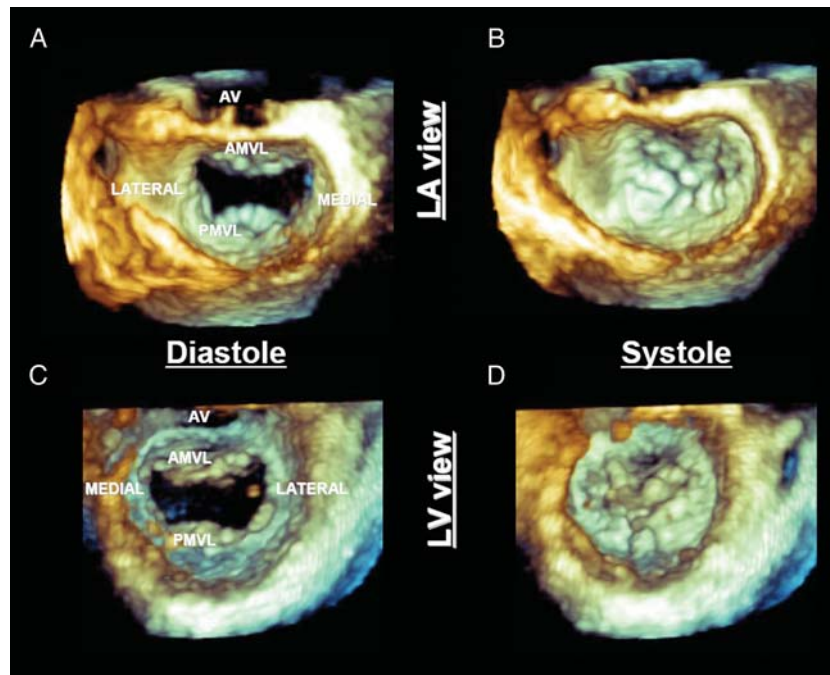


Figure 17 Example of a 3D TEE zoom-mode acquisition of the mitral valve in diastole (**A,C**) and systole (**B,D**) as visualized from the left atrial (LA) (**A,B**) and LV (**C,D**) perspectives. The mitral valve should be oriented with the aortic valve (AV) at the 12 o'clock position irrespective of perspective. AMVL, Anterior mitral valve leaflet; PMVL, posterior mitral valve leaflet.

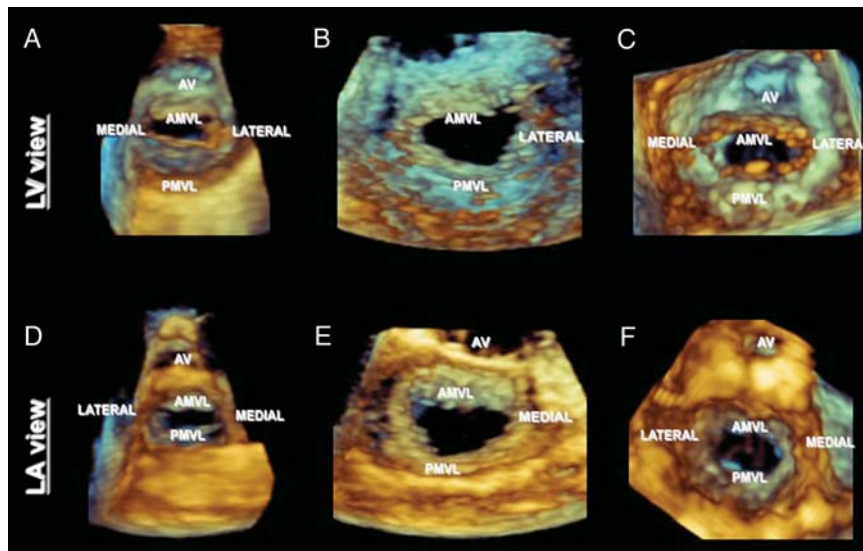


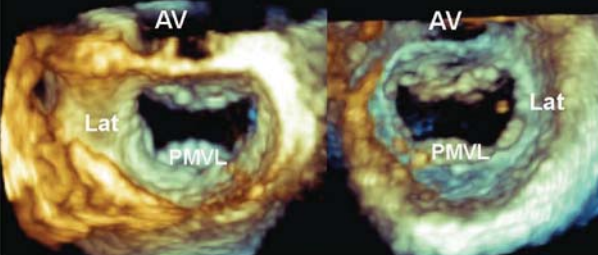
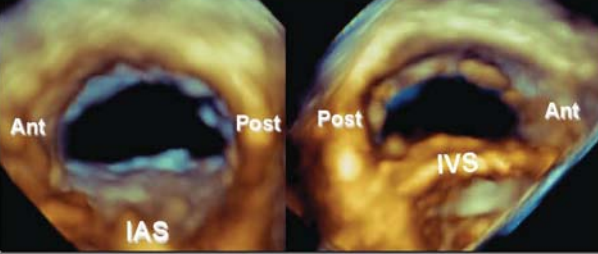
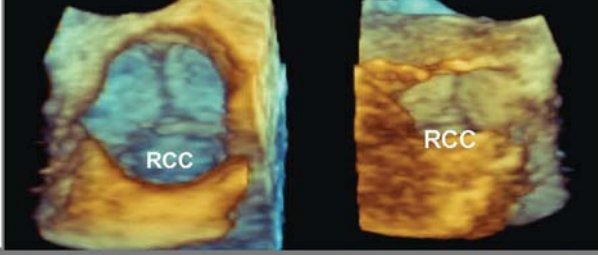
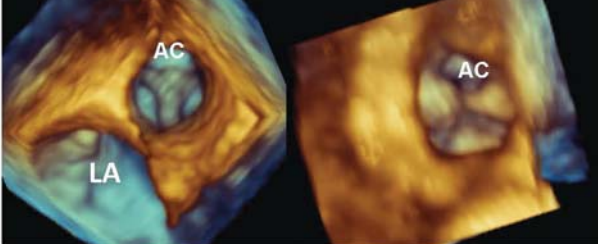
Figure 18 Examples of 3D TTE zoom-mode acquisitions of the mitral valve as visualized from the LV (**A–C**) and left atrial (LA) (**D–F**) perspectives. Note that the mitral valve should be displayed with the aortic valve (AV) at the 12 o'clock position irrespective of perspective. AMVL, Anterior mitral valve leaflet; PMVL, posterior mitral valve leaflet.

chordal insertions on the tips (primary chordae), body (secondary chordae), and base (tertiary chordae) of the mitral valve leaflets. Conversely, chordal rupture with flail or prolapse can be well visualized from left atrial views and/or by selected longitudinal cut planes.

Mitral Annulus

Two-dimensional echocardiography is not able to provide data about mitral annular shape, because mental reconstruction from separate 2D views cannot provide the same information as the volume-rendered 3D reconstruction. Instead, the oval shape of the

Table 6 3DE presentation of cardiac valves

<p>Mitral Valve</p> <p>Display the mitral valve with the aortic valve placed superiorly, regardless if the valve is oriented as viewed from the left atrium or the left ventricle.</p> <p>AV=aortic valve, Lat=lateral left ventricle, PMVL=posterior mitral valve leaflet</p>	<p>Left Atrium</p> <p>Left Ventricle</p> 
<p>Tricuspid Valve</p> <p>Display the tricuspid valve with the septum placed inferiorly in the six o'clock position, regardless if the valve is oriented as viewed from the right atrium or the right ventricle.</p> <p>Ant=anterior, Post=posterior, IAS=interatrial septum, IVS=interventricular septum</p>	<p>Right Atrium</p> <p>Right Ventricle</p> 
<p>Aortic Valve</p> <p>Display the aortic valve with right coronary cusp located inferiorly at the six o'clock position, regardless if the valve is oriented as viewed from the aorta or the left ventricular outflow tract.</p> <p>RCC=right coronary cusp</p>	<p>Aorta</p> <p>Left Ventricular Outflow Tract</p> 
<p>Pulmonic Valve</p> <p>Display the pulmonic valve with the anterior cusp at the 12 o'clock position, regardless if the valve is oriented as viewed from the pulmonary artery or the right ventricle outflow tract.</p> <p>AC=anterior cusp, LA=left atrium</p>	<p>Pulmonary Artery</p> <p>Right Ventricular Outflow Tract</p> 

mitral annulus is best appreciated from the 3DE surgical view of the mitral valve with the entire annular circumference captured in one data set. Moreover, the saddle shape of the mitral valve is best assessed by offline reconstructions, which depict the saddle-shaped contour in three dimensions with high points that are anterior and posterior and low points that are lateral and medial. Commercial software has been developed to precisely quantitate the size, shape, and degree of non-planarity of the mitral valve annulus. This has improved our understanding of mitral valve mechanics. Also, it has assisted surgeons in evaluating the feasibility of mitral valve repair and provided valuable information for annuloplasty ring design.

Left Ventricle

During systole, normal motion and contraction of both the left ventricle and mitral annulus are required to maintain valve competence. Any change in LV geometry that affects papillary muscle position can change the axial relationship of the chordae and leaflets, resulting in poor leaflet coaptation. Three-dimensional transthoracic echocardiography not only allows a qualitative assessment of LV size, geometry, and regional function but also enables comprehensive LV quantitation by several parameters and intuitive display modalities. In addition, dynamic 3D rendering of the mitral valve can discriminate between normal leaflet mobility

and tethered leaflets due to regional wall motion abnormalities or global LV enlargement with increased sphericity (resulting in ischemic or functional mitral regurgitation).

Three-dimensional transesophageal echocardiography can either supplement 3D transthoracic echocardiography, with several unique views and additional information, or replace it, when TTE imaging is impossible (e.g., inadequate acoustic window for 3D echocardiography, intraoperative monitoring).⁸⁷ Also, 3D transesophageal echocardiography has much higher spatial resolution than 3D transthoracic echocardiography, resulting in improved mitral valve anatomic detail. Therefore, assessments of native and prosthetic mitral valve pathology are among the top indications for a 3D TEE exam.²⁴

A comprehensive 2D TEE examination of the entire mitral apparatus still requires numerous probe manipulations, which includes six individual imaging windows while advancing the transducer through three esophageal depths, 180° of multiplane rotation, and an infinite number of probe rotational and flexion maneuvers. Alternatively, 3DE windows acquired with a matrix-array transducer include both area and depth (i.e., volumetric imaging) within the imaging plane. Thus, 3D transesophageal echocardiography requires less probe manipulation and a more efficient examination process.

b. Data Acquisition

Simultaneous Multiplane Mode

This mode allows the mitral valve to be seen in two planes in real-time. The first image is typically a reference, midesophageal four-chamber or five-chamber 2D image of the mitral apparatus, while the second image or “lateral plane” represents a plane rotated 30° to 150° from the reference plane. Multiplane imaging in the elevation plane is also available but not as useful for TEE imaging of the mitral apparatus at the midesophageal depth. Color flow Doppler imaging can also be superimposed onto the 2D images.

Real-Time 3D Mode: Narrow Sector

Live 3D using the matrix-array transducer permits a real-time display of a 30° × 60° pyramidal volume, which is usually insufficient to visualize the entire mitral apparatus in one imaging plane. However, the superior spatial and temporal resolution permits accurate diagnoses of complex pathologies while preserving optimal temporal resolution.

Focused Wide Sector: Zoom

The zoom mode permits a focused, wide-sector view of the mitral valve apparatus from the annulus to the papillary muscle tips. It must be noted that enlarging the region of interest excessively will result in a further detrimental decrease of the temporal resolution. Although this modality allows the entire mitral apparatus to be visualized, rotated, and cropped in real time, enlargement of the sector is at the expense of spatial and temporal resolution relative to real-time 3D echocardiography.

Full Volume: Gated Acquisition

The full-volume mode has the largest acquisition sector possible, which is ideal for imaging the entire mitral apparatus. This mode

also has optimal spatial resolution, which permits detailed diagnosis of complex pathologies. As well, it has high temporal resolution (>30 Hz), which is desirable when diagnosing mechanisms of abnormal mitral leaflet motion. Similar to the real-time 3D and the focused wide-sector zoom modalities, the gated full volume can also be rotated to orient the mitral apparatus in unique en face views from the left atrial and LV perspectives. Furthermore, the full-volume data set can be cropped or multiplane transected to remove tissue planes to identify components of the mitral apparatus within the volume or to visualize 2D cross-sectional x, y, and orthogonal planes using offline analysis software. Color flow Doppler can also be performed in this mode improving assessment of mitral regurgitation jets.

c. Comprehensive Exam

Biplane

The comprehensive 3DE examination of the mitral apparatus begins with a preliminary survey using the 2D multiplane modality while manipulating the lateral plane with and without color flow Doppler to identify the primary mechanism and etiology of mitral valve dysfunction. Thus, biplane imaging could enable the acquisition of an entire 2D multiplane examination of the mitral apparatus at a given esophageal depth.

Real-Time 3D

The size of the real-time 3D sector is usually insufficient to visualize the entire mitral apparatus. Nonetheless, the live 3D pyramidal volume at a decreased depth and appropriate focus can display the mitral valve with more than adequate spatial and temporal resolution to allow an initial rapid 3D assessment of the mitral apparatus. The live 3D mode can display the mitral apparatus en face from either the left atrial or the LV perspective. A real-time 3DE image of the entire left ventricle (increased depth and focus) from the midesophageal five-chamber perspective should also be obtained to view the mitral apparatus in continuity with the LV walls and its association with the coronary sinus. Finally, a real-time 3D view of the mitral apparatus should be obtained from the transgastric two-chamber view to more clearly visualize the papillary muscles and chordae tendineae, which lie more perpendicular to the ultrasound beam compared with their orientation at the midesophageal depth.

Focused Wide-Sector Zoom and Full Volume

Capturing the mitral apparatus in the zoom mode from a midesophageal five-chamber view permits visualization of the mitral apparatus from the annulus to the papillary muscles, with slightly reduced spatial and temporal resolution. The full-volume acquisition of the mitral apparatus using the highest line density and maximum number of individual gated component slabs should always be attempted when ECG gating and the brief acquisition time are permissible, to obtain the most optimal spatial and temporal resolution.

Full Volume with Color Flow Doppler

Color flow Doppler should be added to the full-volume acquisition in patients with mitral regurgitation and/or mitral stenosis. Similar

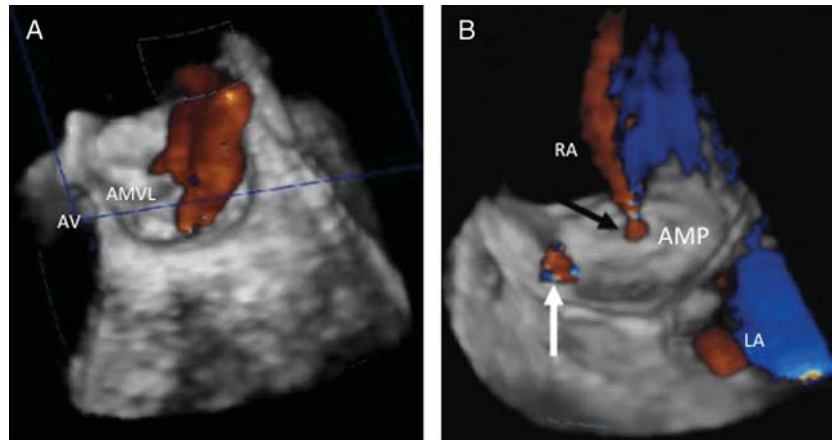


Figure 19 Three-dimensional TEE color Doppler image of mitral regurgitation (left). Three-dimensional TEE color Doppler image of an Amplatzer device after deployment presented as viewed from the right atrium (right). The jet of blood (black arrow) crossing to the right atrium through the center of the device is normal. A residual leak is present (white arrow). AMP, Amplatzer device; AMVL, anterior mitral valve leaflet; AV, aortic valve; LA, left atrium; RA, right atrium.

to the technique for acquiring a wide-sector zoom image, obtaining a 3D color flow Doppler data set initially requires the identification of a region of interest in the orthogonal planes. The size of the region of interest should be limited to the mitral apparatus and color flow Doppler jet to optimize frame rate. In addition, although a high line density may be desirable, a lower line density will permit a larger sector to be displayed. Finally, the largest number of individual gated component slabs (seven to 14) should always be attempted when ECG gating and the brief acquisition time are permissible. Once the full volume with color flow Doppler is obtained, the pyramidal volume can first be viewed as originally obtained from the midesophageal five-chamber view and then rotated to view the mitral apparatus from the left atrial and LV perspectives to identify the sites of jet origin (Figure 19). Further cropping and use of the black-and-white suppress can be used to identify the effective mitral valve orifice and regurgitant orifice areas in patients with mitral stenosis and mitral regurgitation, respectively.

d. Clinical Validation and Application

Evaluation of the mitral apparatus using 3D echocardiography is most useful for (1) defining the extent and location of pathology, (2) determining the mechanism and severity of valvular dysfunction, and, when appropriate, (3) communicating the results of the echocardiographic examination to the interventional cardiologist or cardiac surgeon when an intervention is required. Using the various 3DE modalities described, it is possible to delineate the extent of disease as seen in patients with myxomatous degeneration causing diffuse thickening of the anterior and posterior leaflets with multisegmental prolapse or those with fibroelastic deficiency presenting with focal involvement causing single leaflet prolapse or an isolated flail scallop (Figure 20). These findings have a significant impact on the surgical approach. Perhaps more important, 3D echocardiography may be superior to 2DE techniques and even direct inspection during surgery for diagnosing the location and extent of complex mitral valve disease, especially

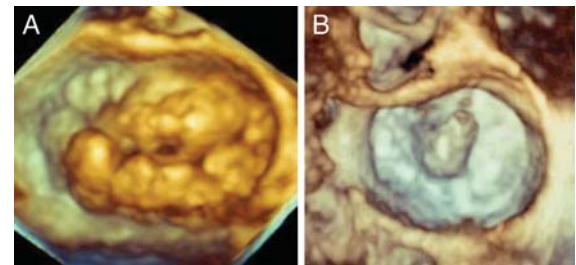


Figure 20 Zoomed 3D TEE view of the mitral valve in patients with Barlow's disease with multisegmental, bileaflet billowing (A) and fibroelastic deficiency with P2 flail segment and ruptured chords (B). Leaflet billowing is diagnosed when there is systolic excursion of the leaflet body into the left atrium due to excess leaflet tissue, with the leaflet free edge remaining below the plane of the mitral annulus. The mitral valve is oriented with the aortic valve at the 12 o'clock position.

when commissural pathology or clefts (Figure 16) are present.^{88–90} The evaluation of mitral prosthetic valve function may also be facilitated with 3DE techniques, especially in identifying the location and severity of perivalvular leaks (Figure 19) and for guiding the positioning of percutaneously placed closure devices.^{91–94}

With improvements in image quality, commercial software has been developed to provide a method for objective quantification of mitral valve changes. Using 3DE data sets, the mitral annulus and leaflets can be traced to create a 3D model of the mitral valve (Figure 21). From these models, volumetric measurements of mitral annular height, mitral leaflet surface area, mitral annular dimensions, and papillary muscle location can be obtained (Figure 22). These dimensions have provided insight into the effects of various mitral valve pathologies and may be useful for directing repair techniques.⁹⁵

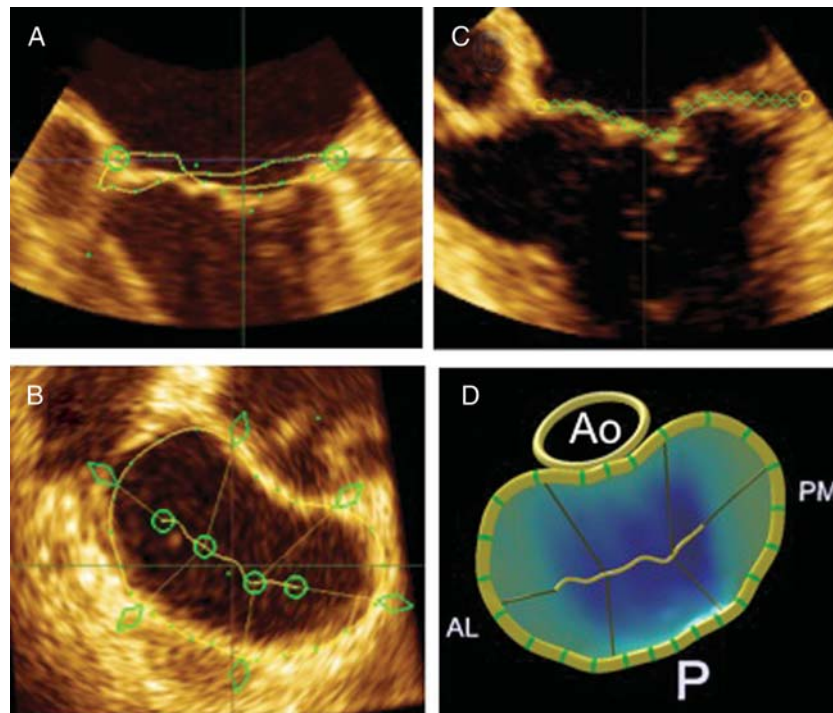


Figure 21 Three-dimensional morphologic analysis of a normal mitral valve. The mitral annulus is manually defined and then repeated in multiple rotational planes (A), yielding a resultant 3D contour superimposed on the en face view of the valve (B). The mitral valve leaflets are then manually traced in multiple parallel planes (C), resulting in a line of coaptation displayed on a color-coded, 3D-rendered valve surface (D). AL, anterolateral; Ao, aorta; P, posterior; PM, posteromedial.

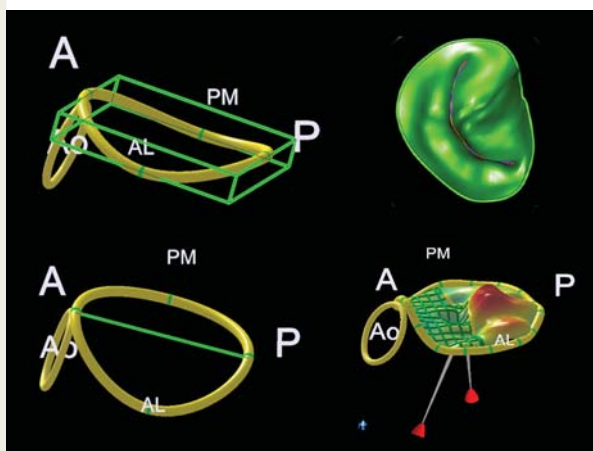


Figure 22 Volumetric quantification of the mitral valve allows accurate measurements of the height of the saddle-shaped mitral valve (top left), commissure-to-commissure diameter measurements of the mitral annulus (bottom left), mitral annular surface area (top right), and the angle between the aortic root and the mitral annulus (bottom right). A, Anterior; AL, anterolateral; Ao, aorta; P, posterior; PM, posteromedial.

Three-dimensional echocardiography is also superior in quantifying mitral stenosis severity, because unlike 2D color Doppler methods such as proximal isovelocity surface area, 3D methods

are independent of the stenotic valve opening angle and the radius of flow convergence (Figure 23). As well, multiplanar reformations from 3DE images can consistently identify the smallest stenotic orifice for area measurements, and these 3DE area measurements are known to correlate strongly with area measurements derived invasively using the Gorlin formula.^{7,96} In contrast, 2D planimetry often overestimates the orifice area when patient image quality is poor or if the narrowest cross-sectional orifice is not properly identified.

In cases of rheumatic mitral stenosis, a 3D echocardiography-based score for percutaneous balloon mitral valvuloplasty has been developed with improved predictive value of success compared with the 2D echocardiography-based Wilkins score.⁹⁷ This improvement was achieved by adding evaluation of the mitral commissural regions to the score and by allowing assessment of individual segments of each leaflet to acknowledge the uneven distribution of anatomic abnormalities in rheumatic mitral stenosis. Most important, the weighting of the individual components of the score were adjusted according to their relative importance in predicting the likelihood of successful percutaneous balloon mitral valvuloplasty.

Because of the complex geometry of the mitral apparatus, 3D echocardiography is uniquely suited for the assessment of mitral regurgitation. Delineation of the effective regurgitant orifice area and the vena contracta are two major strengths of 3D echocardiography. Assessment of the vena contracta area with 3D echocardiography has revealed that it is noncircular in most patients, especially

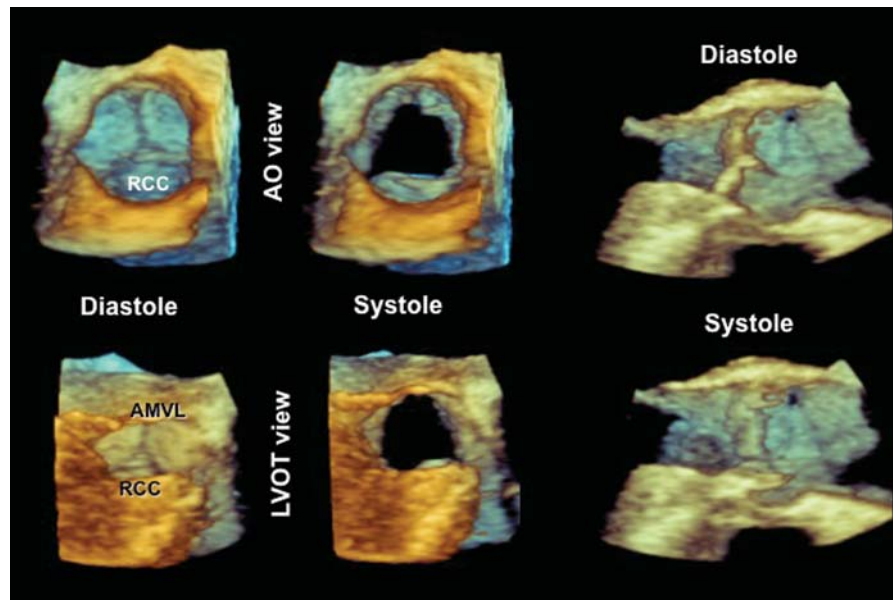


Figure 24 Zoomed 3D TEE image of the aortic valve as seen from the ascending aorta (Ao) in diastole (*top left*) and systole (*top middle*) and from the LV outflow tract (LVOT) in diastole (*bottom left*) and systole (*bottom middle*). Note that the aortic valve is oriented with the right coronary cusp (RCC) located inferiorly irrespective of the perspective. The 3D TEE data set is cropped to display the aortic valve in long-axis form during diastole (*top right*) and systole (*top, left*). LCC, Left coronary cusp; NCC, noncoronary cusp.

by the corresponding presence or absence of the coronary arteries (left coronary, right coronary, and noncoronary cusps) (Figure 24). Each semilunar cusp is attached to the aortic wall in a curved manner, with the basal attachment located in the left ventricle below the anatomic ventriculoaortic junction and the distal attachment at the sinotubular junction.⁹⁹ The sinuses of Valsalva and the sinotubular junction are integral parts of the valvular mechanism, such that any significant dilatation of these structures will result in aortic valve incompetence. Overall, when tracking the curved path of the aortic leaflet insertion points, the 3D spatial configuration of the aortic valve resembles a crown.

The common approaches for imaging the aortic valve by 3D transthoracic echocardiography are from the parasternal and apical views. Three-dimensional data sets including the aortic root can be cropped and rotated for a dynamic 3D rendering of the aortic valve, which can be visualized from both the aortic and ventricular perspectives, as well as sliced in any desired longitudinal or oblique plane. The aortic perspective of the valve is best suited for assessing valve morphology, while the ventricular perspective may best delineate aortic tumors or vegetations or subvalvular obstructions.

An exact en face alignment of the cut plane to the aortic valve orifice is sometimes impossible to obtain in the 2D short-axis view, especially in hearts with aortic root pathology or a horizontal position. In addition, the through-plane motion of the aortic annulus throughout the cardiac cycle due to the active longitudinal excursion of LV base often hampers adequate visualization of the true aortic valve opening orifice and morphology throughout the cardiac cycle. With three-dimensional echocardiography, en face alignment of the cut plane to the aortic annulus orifice is easily

obtained, irrespective of the actual spatial orientation of the aortic root in the body. Moreover, the 3D en face view allows comprehensive visualization of the entire aortic valve complex in motion. Three-dimensional echocardiography also provides additional information on the spatial relationship with surrounding structures, such as the LV outflow tract and mitral annulus, without the need for the cumbersome mental reconstruction applied with 2D echocardiography.

The 2DE parasternal long-axis view of the aortic valve and root often underestimates LV outflow tract area, as it presumes a circular shape. Three-dimensional echocardiography enables multiplane imaging of the aortic valve (e.g., simultaneous display of the valve in both the long and short axes), demonstrating the true shape of the LV outflow tract. As well, 3D echocardiography often confirms normal and abnormal findings when structures visualized in one plane can be examined in real time by checking a second orthogonal plane.

The apical approach allows the en face visualization of the aortic valve by 3D echocardiography when the parasternal approach is inadequate. Even though the spatial resolution is lower compared with the parasternal approach, an accurate assessment of the aortic valve morphology (number of cusps and mobility, opening orifice, regurgitant orifice) and LV outflow tract anatomy is possible from apical images. Gain and thresholding adjustments ensure an accurate delineation of the aortic valve anatomic details, while the addition of various color maps increases the depth perception in three dimensions. However, adequate visualization can be at times difficult by transthoracic 3D echocardiography either in normal (with very thin cusps, leading to significant drop-out of the leaflet bodies) or in heavily calcified

be located superiorly in the 12 o'clock position irrespective of perspective (Tables 4 and 6).

Focused Wide-Sector Zoom and Full Volume

The zoom mode image of the pulmonary valve allows visualization of the pulmonary valve leaflets as well as the main pulmonary artery and the RV outflow tract. Once the pyramidal volume is captured, the en face view of the valve can be displayed. As well, the cropping plane can be used to assess the dimensions of the main pulmonary artery and the RV outflow tract.¹¹⁵ Last, the cropping plane can be used to show the RV outflow tract, pulmonary valve, and main pulmonary artery in a single image.

Full Volume with Color Flow Doppler

In patients with pulmonary regurgitation or stenosis, color flow Doppler should be added to the full-volume acquisition. The size of the region of interest should be limited to the pulmonary valve and the color flow Doppler jet to optimize frame rate. As mentioned previously, the largest number of individually gated component slabs should always be attempted when ECG gating and brief acquisition times are possible. Once acquired, the pyramidal volume can first be viewed as originally obtained and then rotated to view the pulmonary valve from the pulmonary artery and right ventricle to identify the site of jet origin. Further cropping and the use of the black-and-white suppress can be used to identify effective orifice area, regurgitant orifice area, 3D proximal isovelocity surface areas, and vena contracta.

c. Clinical Validation and Application

Evaluation of the pulmonary valve using 3D echocardiography has been shown to be most useful for defining the location of pathology and determining the mechanism and severity of valvular dysfunction. Using the modalities available with 3D echocardiography, cusp number, thickness, and mobility can be determined in patients with congenital pulmonary valve diseases and disease processes such as carcinoid valvulopathy, endocarditis, and so on. Additionally, 3D echocardiography provides accurate RV outflow tract supra-valvular, subvalvular, and valvular measurements in patients with congenital RV outflow tract obstruction. Most importantly, 3D echocardiography improved the accuracy in the assessment of pulmonary regurgitation, which has implications in determining the timing of surgical intervention.¹¹⁶

There is no current evidence supporting the routine use of 3D transthoracic echocardiography or transesophageal echocardiography for the evaluation of pulmonic valve disease.

14. Tricuspid Valve

a. Anatomy and Limitations of 2DE Assessment

The TV is composed of the annulus, leaflets, and chordal and papillary muscle apparatus. The tricuspid annulus consists of a fibrous ring from which the leaflets are suspended. The normal tricuspid annulus area measures between 8 and 12 cm² and is approximately 20% larger than the mitral annulus. Three-dimensional

echocardiographic assessment of the tricuspid annulus has demonstrated that the tricuspid annulus is bimodal in shape (saddle shaped) with higher or superior points (toward the right atrium) along the anterior and posterior aspects of the annulus and the low or inferior points (toward the right ventricle) along the medial and lateral aspects of the annulus.^{117–119}

The TV, as its name implies, has three leaflets, designated anterior, septal, and posterior. The anterior tricuspid leaflet has the largest leaflet area and is attached along the anterolateral (free wall) surface of the tricuspid annulus. The septal leaflet attaches along the interventricular surface and the posterior leaflet along the posterior portion of the annulus. Embryologically, the septal and posterior leaflets arise from the same endocardial cushion bud, but a cleft forms dividing into the septal and posterior leaflets. Tricuspid leaflets are also thinner and more translucent than the mitral valve.

The tricuspid apparatus has two main papillary muscles, located anteriorly and posteriorly, and frequently a third one arising from the infundibulum (conus or RV outflow tract). Chords from each papillary muscle attach to all three tricuspid leaflets.

b. Data Acquisition

Two-dimensional echocardiographic imaging of the TV requires reconstruction from multiple planes.¹²⁰ Three-dimensional TTE imaging of the TV allows visualization of all aspects of the TV from a single full-volume data set or a focused examination on a particular TV aspect using a narrower imaging acquisition mode with higher resolution.^{120–122} Three-dimensional TTE imaging can be limited by relatively low temporal resolution compared with 2D echocardiography.

c. Orientation and Display

With 3D echocardiography, it is possible to display the valve in a manner that is not possible using standard 2D echocardiography. Such an example is the en face view of the TV visualized from either the right atrial or RV perspective (Figure 14). When displaying the TV en face, the septal leaflet should be located in the 6 o'clock position irrespective of perspective (Tables 4 and 6). These en face views may be especially helpful in localizing leaflet disease such as leaflet prolapse, perforation, or vegetation, as well as localizing the origin of regurgitation jets, or planimetry the tricuspid orifice area to assess severity of tricuspid stenosis.^{121,122} In addition to standard views, the cropping plane can be adjusted to visualize a particular section of the TV.

d. Analysis Methods

Cropping methods can be performed in a standardized manner to produce similar views for display. Standard 3DE data sets to crop into should be obtained from parasternal and apical windows. A subcostal 3DE data set can also be acquired but will depend on the image quality of the subcostal window. The full-volume data set should be optimized to view the TV and the right ventricle. Once cardiac structures are visualized with the cropping plane, the image display can be optimized using the gain, compress, and magnification settings.

Parasternal Views

The TV in the RV inflow view should be optimized for 3D full-volume data acquisition. The cropping plane should crop into the data set oriented to display the anterior and posterior leaflets of the TV. In most views, this should also display the orifice of the coronary sinus and Eustachian valve (if present). A second parasternal data set should be acquired with the TV with the RV outflow tract and aortic valve in the short axis.

Apical Views

The cropping plane should crop into the data set along the coronal plane to obtain a four-chamber view of the TV with anterior and septal leaflets in view and its chordal attachments. Then, the cropping plane should be oriented along the sagittal plane to visualize the posterior and anterior leaflets of the TV. Finally, the cropping plane should be rotated (45°) clockwise to include the aortic valve. This maneuver should allow visualization of the septal leaflets and anterior leaflets of the TV.

Transverse Views

The cropping plane should crop into the data set from the right atrium in the transverse plane. A similar view can be obtained cropping from the right ventricle to visualize the RV aspect of the TV and subvalvular apparatus.

e. Clinical Validation and Application

Three-dimensional echocardiographic of the TV has provided insights into normal and abnormal TV anatomy.^{121,122} In a study of 29 patients with a spectrum of TV pathologies, 3D echocardiography provided incremental diagnostic value over 2D echocardiography with regard to the etiology and location of the abnormal leaflet segments.¹²³ Three-dimensional echocardiography has demonstrated that the TV annulus has a bimodal or saddle shape with distinct high (superior) points oriented anteriorly and posteriorly and low (inferior) points oriented medially and laterally.¹¹⁷ The bimodal shape is similar to that of the mitral valve annulus. With the development of functional tricuspid regurgitation, the tricuspid annulus becomes more planar, and also more circular, expanding mostly along the anterolateral border.^{117,118}

In descriptive studies, 3D echocardiography has provided mechanistic insights into tricuspid regurgitation in patients with pulmonary hypertension⁷⁰ and congenital heart disease.^{124–126} In a study of 87 patients with pacemakers or implantable cardioverter-defibrillator leads, 3D echocardiography identified the lead position as it traverses the TV, resulting, at times, in tricuspid regurgitation.¹²⁷

3. Color Tricuspid Regurgitation

There are few data on 3D color Doppler assessment of tricuspid regurgitation. A recent article by Velayudhan et al.¹²⁸ demonstrated efficacy in measuring the vena contracta of the tricuspid regurgitant jet using 3D color Doppler data. Figure 14 shows an example of the use of color 3D echocardiography to guide vena contracta measurements. The concept of 3D-guided measurement of the vena contracta area to quantitative tricuspid regurgitation has advantages over 2D color Doppler assessment, as it does not require geometric assumptions or reliance on the distant jet

for quantification. However, 3D color Doppler temporal resolution is low compared with 2D, and the ability to measure the vena contracta area may have technical limitations in individual patients. The use of 3D to assess tricuspid regurgitation is likely to increase as more experience is gained and technological advances are made.

There is evidence supporting the routine use of 3D transthoracic echocardiography or transesophageal echocardiography for the evaluation of TV disease.

15. Right and Left Atria

a. Anatomy and Limitations of 2DE Assessment

The rapid development of cardiac electrophysiology has triggered renewed interest in the anatomy of atrial cavities and their target structures. Although fluoroscopy is routinely used to localize atrial anatomic landmarks during electrophysiologic procedures, this technique is limited by its 2D projection of complex 3D structures that may render difficult interpretation and analysis, and specific atrial structures such as the fossa ovalis, crista terminalis, Eustachian valve, coronary sinus ostium, and pulmonary vein ostia may be difficult to visualize. Thus, a preprocedural assessment of the various atrial landmarks involved in electrophysiologic procedures may have clinical relevance, providing electrophysiologists with a useful preprocedural anatomic “roadmap.”¹⁷ Because the atria are close to the esophagus, 3D transesophageal echocardiography provides fine anatomic data of internal atrial structures, as recently shown.¹²⁹

The cross-sectional approach has been for a long time and remains the most common way of displaying echocardiographic images. Using 3D transesophageal echocardiography, the same anatomic structures may be imaged from countless perspectives. Thus, for discrete atrial landmarks, rather than a “cross-sectional” approach, a “structure-oriented” approach should be used. Once a specific anatomic target has been identified (usually using a zoom modality, biplane oriented), the volume data set can be cropped, expanded, and oriented to obtain the most effective perspective.

Right Atrial Anatomy

The right atrium consists of four components, the right atrial appendage, the venous part, the vestibulum, and the atrial septum, which is shared with the left atrium. However, specific anatomic structures such as the crista terminalis, cavotricuspid isthmus, Eustachian valve, coronary sinus ostium, and fossa ovale, are of particular interest because they are targets for catheter-based procedures.

Crista Terminalis

An external fat-filled groove, the sulcus terminalis, divides the venous part of the atrium from the right atrial appendage (the true primitive atrium). The sinus node is located in this groove close to the superior cavoatrial junction. The sulcus terminalis corresponds internally to the crista terminalis, which is a roughly C-shaped muscular band separating the smooth wall of the

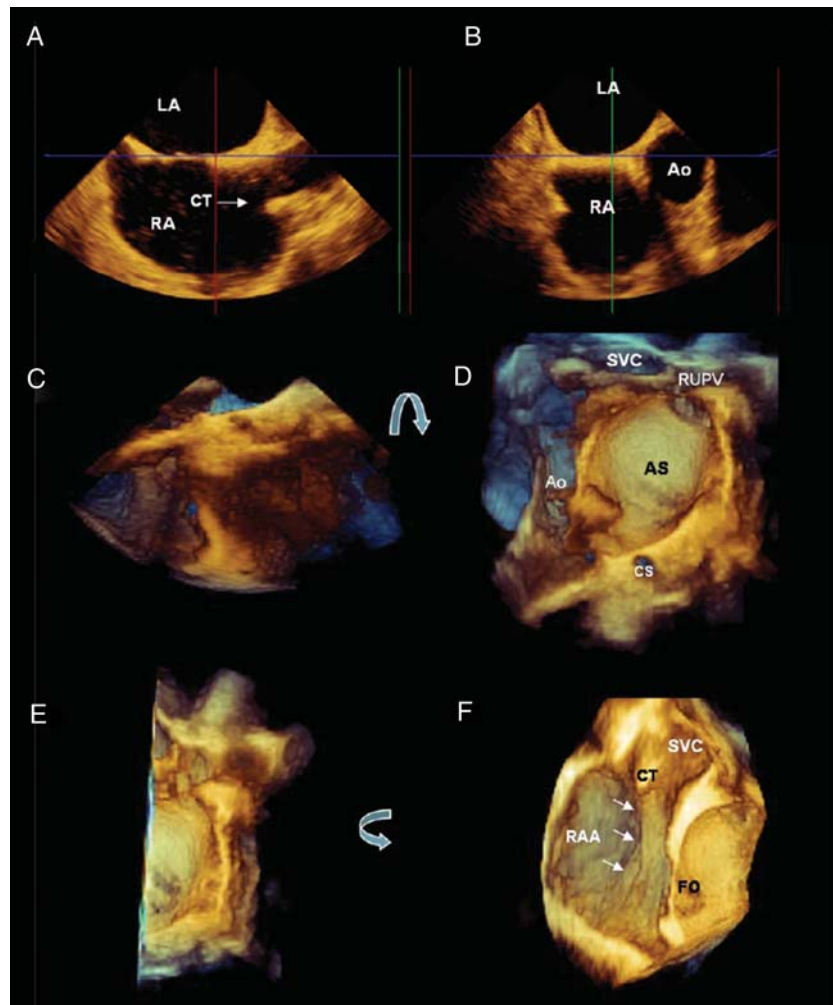


Figure 26 Still image depicting the two perpendicular 2D TEE planes (**A,B**) used to acquire a zoomed 3D TEE data set of the interatrial septum (**C**). The left side of the atrial septum (**AS**) in shown in the en face perspective visualized after a 90° up-down rotation (*curved arrow*) of the data set (**D**). Image **D** can be cropped to remove the left half of the atrial septum (**E**), and when rotated 90° counterclockwise (*curved arrow*), the entire course of the crista terminalis (**CT**) from the superior vena cava (**SVC**) toward the inferior vena cava (*arrows*) can be visualized, as seen in image **F**. Ao, Aorta; CS, coronary sinus; FO, fossa ovalis; LA, left atrium; RA, right atrium; RAA, right atrial appendage; RUPV, right upper pulmonary vein.

venous component from the rough wall of the right atrial appendage.¹³⁰ Pectinate muscles emerge from the crista terminalis, spreading out into the right atrial appendage. The crista may vary in size and thickness, appearing as a small, thin, valvelike or a broad-based structure. A very large crista terminalis mimicking a mass can be found in so-called lipomatous hypertrophy of atrial septum, which is caused by an extensive fatty infiltration of the sulcus terminalis. The crista terminalis is an area of marked anisotropy, and almost two thirds of focal right atrial tachycardias occurring in the absence of structural heart disease arise along the crista terminalis¹³¹ and, occasionally, are the target for catheter ablation. Because the crista terminalis originates from the superior vena cava dividing the right atrial appendage from the sinus, both the superior vena cava and right atrial appendage are useful landmarks to localize the crista terminalis.²² When the crista terminalis has a broad-based insertion, one of the easiest methods for imaging

the entire course of the crista terminalis from right perspective is depicted in Figure 26.

Cavotricuspid Isthmus and Surrounding Structures

The cavotricuspid isthmus is a well-defined region of atrial tissue that is related to the origin of typical atrial flutter. The cavotricuspid isthmus is a roughly quadrilateral-shaped atrial wall bordered by the tricuspid hinge line anteriorly and by the Eustachian valve posteriorly. The inferior border of the ostium of the coronary sinus lines the superomedial border, while the inferolateral border is delineated by the final ramification of the crista terminalis.¹³² In normal hearts, the topography of the cavotricuspid isthmus is not flat. Usually a slight depression (sub-Eustachian pouch or sinus of Keith) between the Eustachian ridge and the TV can be found. In some individuals, this pouch may be deeper than normal or even aneurysmal. The Eustachian valve is a semilunar flap of fibrous or fibrous-muscular tissue

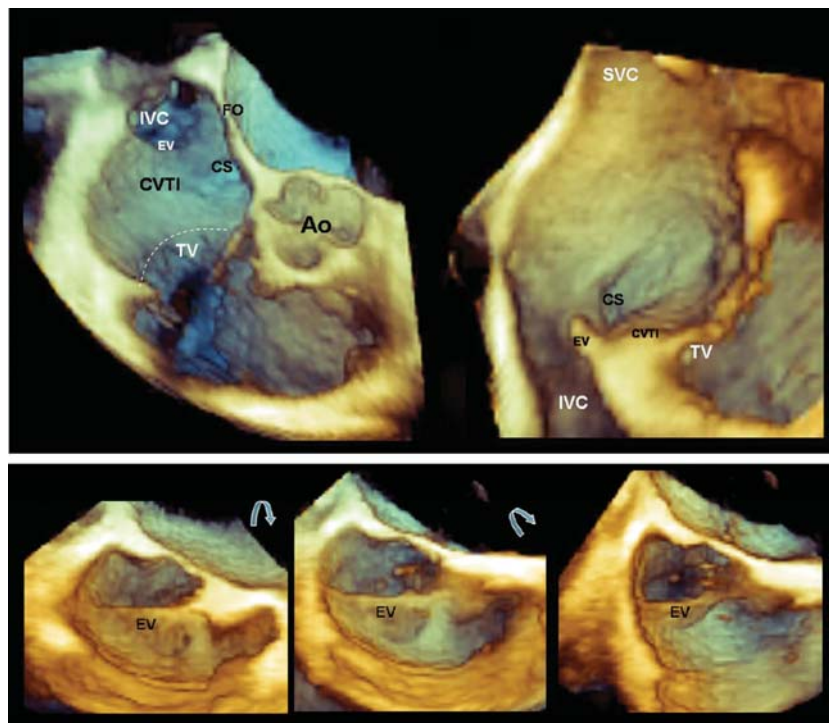


Figure 27 Three-dimensional TEE en face image of the cavotricuspid isthmus (CVTI) (*top right*), which is similar to the fluoroscopic left anterior oblique projection. A view perpendicular allows visualization of the CVTI from the Eustachian valve (EV) insertion point to the white dots demarcating the TV hinge line (*top left*). Magnified 3DE en face image of the EV (*bottom left*) in which the superior border of the valve is well defined. With slight rotation, the inferior border can be visualized (*bottom middle and right*). Ao, Aorta; CS, coronary sinus; FO, fossa ovalis; IVC, inferior vena cava; SVC, superior vena cava.

variably developed that guards the entrance of the inferior vena cava. The Eustachian valve continues medially with a muscular band called the Eustachian ridge. This latter delineates the border between the fossa ovalis and the ostium of the coronary sinus. Occasionally, the Eustachian valve may be very prominent. The coronary sinus ostium is the entrance of the coronary sinus and a flap of thin fibrous tissue called the Thebesian valve guards it. Because the cavotricuspid isthmus is not a specific structure but a muscular region of right atrial cavity bordered by well recognizable anatomic landmarks, imaging these structures can draw the virtual perimeter of the cavotricuspid isthmus. Simultaneous visualization of the posterior tricuspid hinge line, the Eustachian valve, and the ostium of the coronary sinus can be obtained when focusing on the atrial cavity, regardless of the initial cut plane used (four-chamber, basal short-axis, or bicaval view). The ostium of coronary sinus is located medially to the Eustachian valve and can be visualized by a 90° clockwise rotation from the four-chamber cut (Figures 27 and 28).

The fossa ovalis is a relevant anatomic landmark important to identify when performing transseptal punctures for left-sided catheter-based procedures and left pulmonary vein ablation. The size, location, and topography of the fossa ovalis may vary from heart to heart. The fossa ovalis is a depression in the right side of the atrial septum. At the left side, the septum primum covers this region and is usually featureless. The fossa ovalis actually represents the “true” atrial septum in the sense that it directly

divides the two atrial chambers. The majority of the remaining tissue that separates the atrial chambers is composed of an infolding of the atrial wall with fibrofatty tissue that extends from the epicardium.¹³³ Imaging of the fossa ovalis is usually obtained from a 2D TEE bicaval plane view. The depth of pyramidal data set should be adjusted to include only the left and the right sides of the atrial septum. This specific setting allows the entire septum to be acquired in 3D format without surrounding structures. With a 90° up-down angulation of the pyramidal data set, the entire left-sided aspect of the septum is shown in an “en face perspective” (Figure 29). Once the left side of the atrial septum is acquired, a 180° counterclockwise rotation shows the right side of the atrial septum and the fossa ovalis as a depression on the septum (Figure 30). Sometimes a fine cropping using the arbitrary crop plane is necessary to remove those surrounding atrial structures that may cover the septum. A gain setting at medium level is usually required to avoid disappearance of the fossa ovalis and creating a false image of an atrial septal defect.

Left Atrial Anatomy

The left atrium consists of three parts: the appendage, the vestibule, and the venous component. The left atrial appendage is a multilobar structure located between the left upper pulmonary vein and the left ventricle. The vestibule is the part of the left atrium that surrounds the mitral valve orifice and has no distinctive

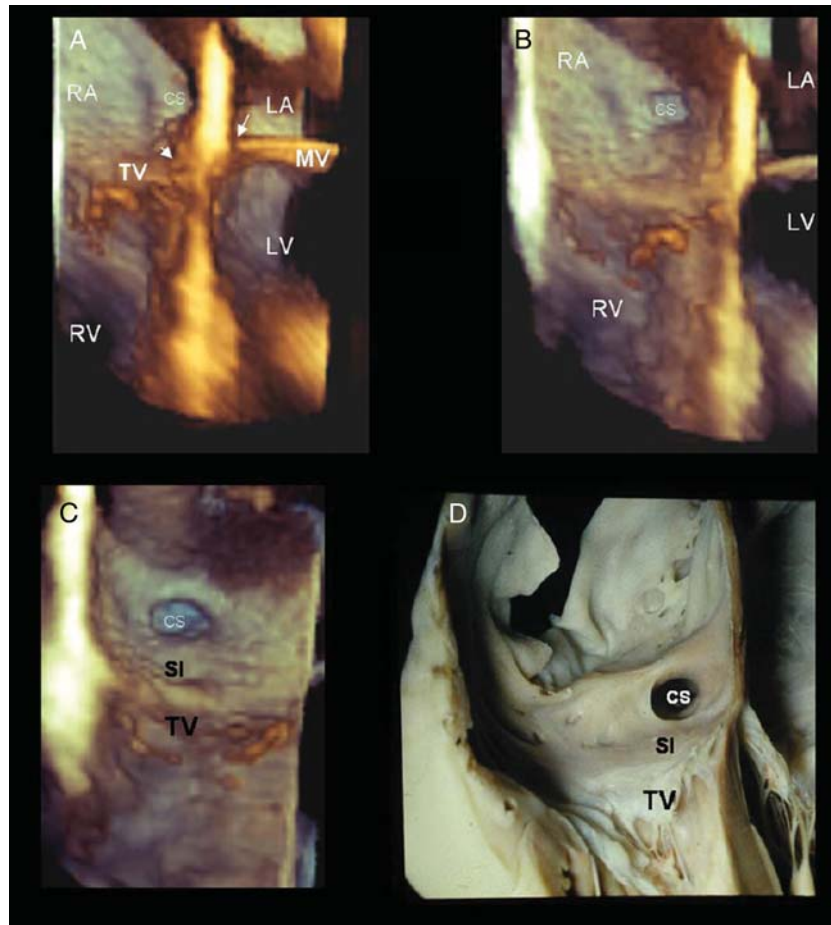


Figure 28 Three-dimensional TEE image of the crux cordis, which is the cross-shaped intersection between the atrial and ventricular septal planes and the plane of the atrioventricular junction (**A**). With slight rotation of the image to expose the right side of the atrial septum, the ostium of the coronary sinus (CS) becomes more visible (**B**), and the septal isthmus (SI) (**C**), the region between the inferior border of CS and the hinge line of the TV, can be visualized. Image **D** is a photograph of an anatomic specimen presented in a view similar to the image in **C**. LA, Left atrium; LV, left ventricle; MV, Mitral valve; RA, right atrium; RV, right ventricle.

anatomic characteristics. The pulmonary veins drain oxygenated blood from the lung into the left atrium through oval-shaped ostia. Although there is significant variability in the dimensions, shape, and branching patterns of the pulmonary veins, the most common pattern of entry is two veins from the hilum of each lung. The superior pulmonary vein ostia tend to be larger and have longer distances from the ostium to the first-order branches than the inferior veins. The right superior pulmonary vein lies just behind the superior vena cava. The left pulmonary veins are separated from the left atrial appendage by the ligament of Marshall.

b. Data Acquisition

Biplane Imaging

A preliminary survey of the left atrium can be performed using the 2D multiplane modality while manipulating the lateral plane with and without color flow Doppler to identify the pulmonary veins.

Real-Time 3D

Overall, acquisition of the left atrium for volume and function measurements should be from TTE views or TEE transgastric views (Tables 2 and 3). With midesophageal TEE views, the entire left atrium cannot be seen within the imaging pyramid, precluding measurements of left atrial volumes. As well, 3D transesophageal echocardiography cannot visualize the entire atrial posterior wall with all four pulmonary veins. However, it can provide high-quality images of one or two of the pulmonary vein ostia and surrounding left atrial tissue. Three-dimensional transesophageal echocardiography is ideal for visualization of the interatrial septum and its adjacent structures (Figure 31).

From the midesophageal 90° TEE view of the mitral valve and left atrial appendage with a slight counter clockwise rotation, one or both of the left pulmonary veins can be displayed. Once the 2D TEE image is optimized, narrow-angled acquisitions can be used to optimize the 3D image (Figure 31). Because the two left pulmonary veins have different directions, slight up-and-down manipulations of the TEE transducer may be required to maximize

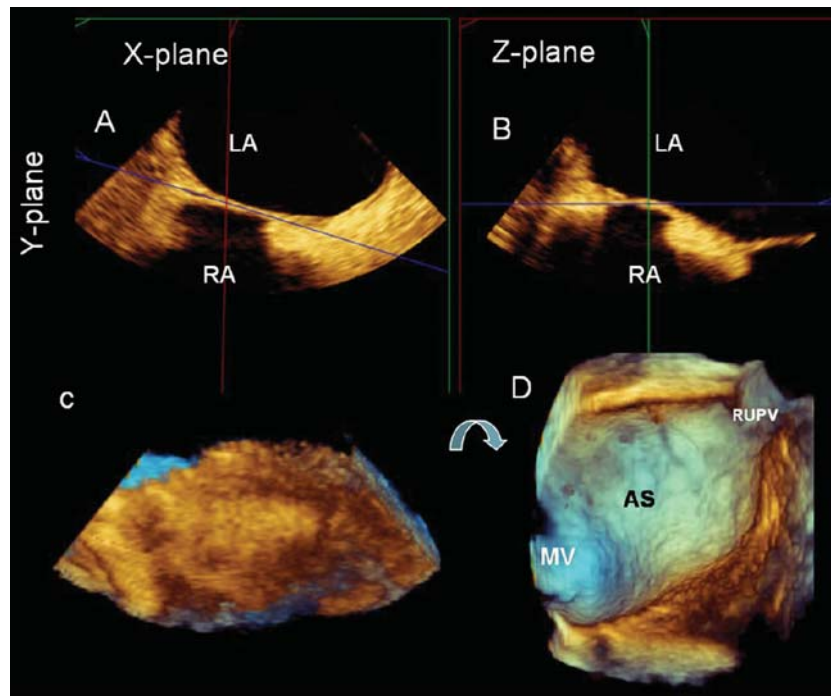


Figure 29 Composite image showing the two perpendicular planes on 2D transesophageal echocardiography (A,B) used to acquire zoomed 3D TEE data set of the atrial septum (AS) (C). Note that the sector dimension is larger in the x and z directions and shorter in the y direction. These settings allow the interatrial septum to be acquired in high resolution excluding right atrial structures that may mask the right aspect of the septum. A 90° up-down rotation (curved arrow) of the pyramidal data set allow the left atrial side of the AS to be viewed (D). LA, Left atrium; MV, mitral valve; RA, right atrium; RUPV, right upper pulmonary vein.

visualization of the ostia of the superior or inferior pulmonary vein, respectively.

From the midesophageal view of the left pulmonary veins, a clockwise rotation depicts the entire atrial septum en face. This image can be rotated to display it from the left or right atrial perspectives. The right pulmonary veins appear in the long-axis orientation. With a slight down-to-up angulation, the ostia of both right pulmonary veins become visible.

Focused Wide-Sector Zoom and Full Volume

Once a wide-angled acquisition 3D data set of the septum is obtained, the cropping plane can be used to optimize views of the septum, demonstrating its relationship to structures such as the mitral valve, right upper pulmonary vein, and aorta (Table 5). As well, the cropping planes can be aligned perpendicular to the pulmonary vein orifices to obtain ostial dimensions (Figure 32).

Full Volume with Color Flow Doppler

Color Doppler 3D imaging should also be performed to assess flow in the pulmonary veins.

Transthoracic Echocardiography

To assess right and left atrial volumes, the data set should be acquired from an apical approach, taking care to encompass the entire atrial cavities. Sometimes (e.g., in enlarged atria) separate

dedicated acquisitions are needed to be able to acquire the whole right or left atrium.

c. Clinical Validation and Application

Three-dimensional transthoracic echocardiography has been used to assess left atrial volumes in patients undergoing radiofrequency catheter ablation of atrial fibrillation.^{134–136} Volumes obtained from 3D echocardiography were smaller than on angiography and electroanatomic mapping. These results suggested that left atrial volumes obtained by angiography or electroanatomic mapping should not be used as baseline values for noninvasive follow-up. As well, these studies also demonstrated that left atrial volumes and function improves if sinus rhythm is maintained after ablation.

There is promise that 3D transthoracic echocardiography will improve the accuracy of left atrial volume measurements. However, no studies to date have evaluated right atrial volumes.

16. Left Atrial Appendage

a. Anatomy and Limitations of 2DE Assessment

The left atrial appendage is a long, tubular, multilobar structure that is usually heavily trabeculated with muscular structures, the so-called pectinate muscles. The left atrial appendage orifice is

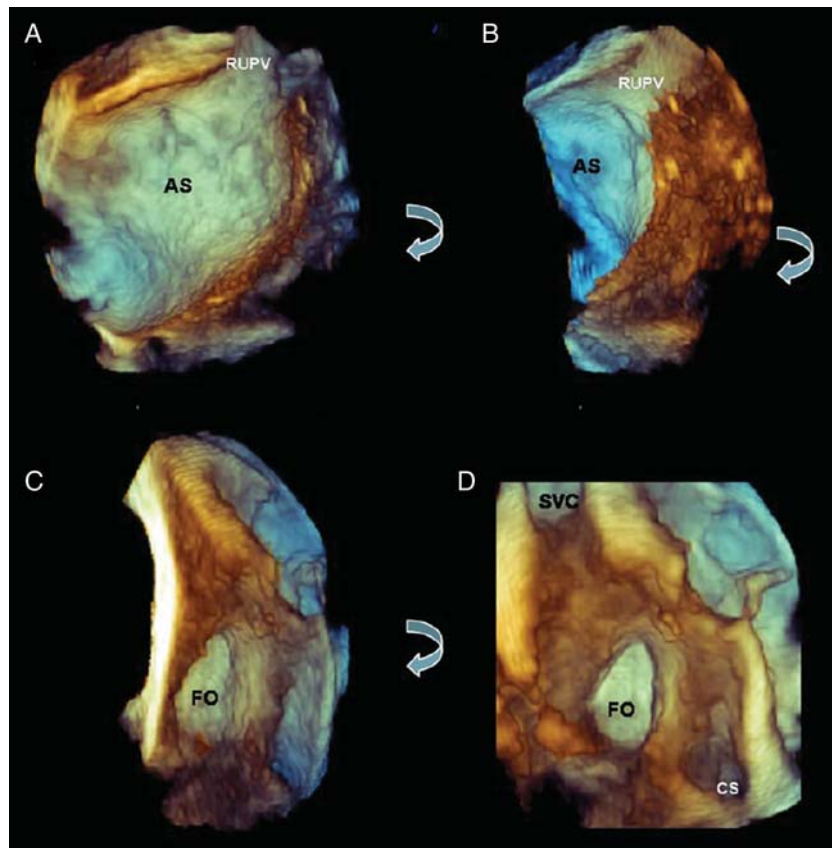


Figure 30 Three-dimensional TEE image of the left atrial septum (AS) oriented with the right upper pulmonary vein (RUPV) located superiorly (A). Progressive rotation of this image following the curved arrows (B) reveals the crater-shaped fossa ovalis (FO) (C) and the entrance of the superior vena cava (SVC) and coronary sinus (CS) (D).

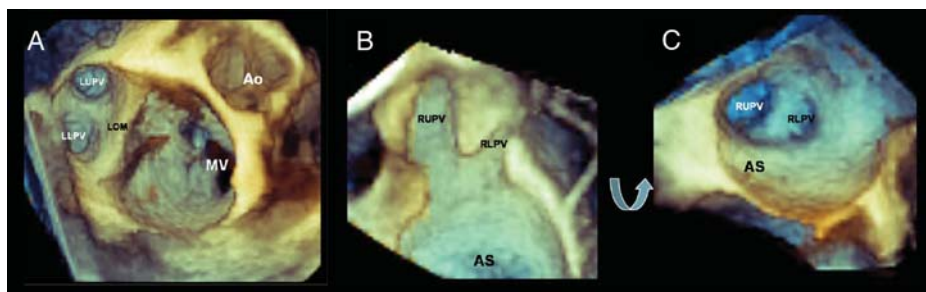


Figure 31 Three-dimensional TEE image of the left upper pulmonary vein (LUPV) and left lower pulmonary vein (LLPV) (A). Slight angulation makes it possible to visualize both ostia simultaneously. Three-dimensional TEE image of right upper pulmonary vein (RUPV) and right lower pulmonary vein (RLPV) in long-axis (B) and short-axis (C) orientations. Ao, Aortic valve; AS, atrial septum; LOM, ligament of Marshall; MV, mitral valve.

located between the left upper pulmonary vein and the left ventricle and extends anteriorly over the atrioventricular (coronary) sulcus.^{137,138} The orifice separates the trabeculated walls of the left atrial appendage from the smooth walls of the left atrium (Figure 32).¹³⁹ The circumflex branch of the left coronary artery

runs close to the left atrial appendage basal orifice. The cardiac lymphatic drainage of the left ventricle is thought to pass beneath the left atrial appendage.^{137,140} Studies has demonstrated great variability in left atrial appendage volume, length, principal-axis angle, and orifice diameter.^{139,141,142}

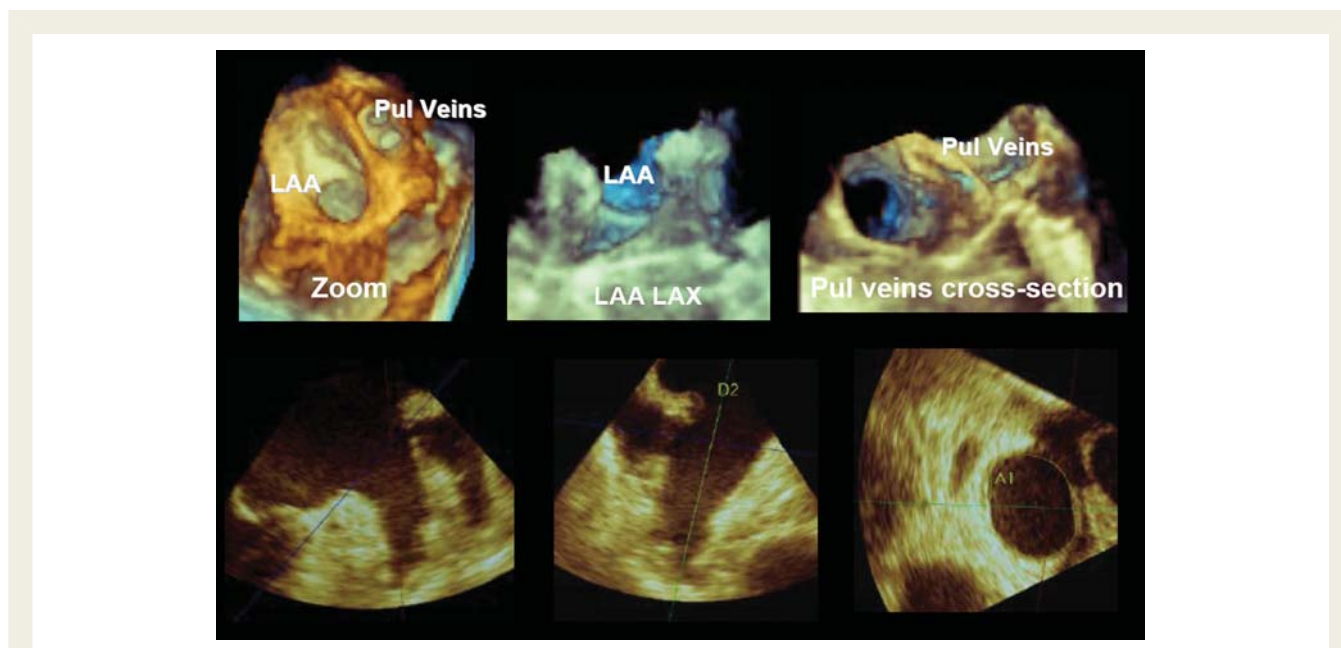


Figure 32 Zoomed 3D TEE image of the left atrial appendage (LAA) orifice as viewed from the left atrium (*top left*) and of the complete appendage in long axis (LAX) (*top middle*). From the 3DE data set, two orthogonal LAX 2D planar views of the left atrial appendage can be displayed (*bottom left and middle*) as well as a short-axis view (*bottom right*). Zoomed 3D TEE image of the pulmonary (Pul) veins in cross-section (*top left*). A, Area; D, dimension.

b. Data Acquisition and Display

Biplane Imaging

Two-dimensional multiplane imaging of the left atrial appendage can be performed from a single view of the left atrial appendage at 0°, 45°, 90°, or 135°. Manipulation of the lateral plane allows identification of the left atrial appendage lobes.

Real-Time 3D

From the 0°, 45°, 90°, or 135° 2D TEE views of the left atrial appendage, narrow-acquisition 3D images can be used to optimize gain settings (Table 3).

Focused Wide-Sector Zoom and Full Volume

On zoom-mode images, the cropping plane can be used to obtain an en face view of the left atrial appendage orifice that can be measured. As well, the planes can be adjusted to obtain left atrial appendage depth. Table 5 describes the presentation of the left atrial appendage.

c. Clinical Validation and Application

Three-dimensional echocardiography plays an important role in percutaneous closure of the left atrial appendage. Three-dimensional echocardiography has been shown to be superior to 2D transesophageal echocardiography in discriminating between left atrial appendage pectinate musculature and thrombus in patients with atrial fibrillation.¹⁰⁰ As well, to determine device size, accurate left atrial appendage orifice area is needed. Studies have shown that 3D TEE measurements from the en face view of left atrial appendage orifice area correlate well with computed

tomographic values, while 2D transesophageal echocardiography underestimated left atrial appendage orifice area. Importantly, 3DE imaging allows the left atrial appendage to be well visualized before, during, and after the procedure.

17. 3D Stress Echocardiography

Three-dimensional stress echocardiography represents a major advancement for the evaluation of ischemic heart disease. It has been performed with exercise,^{143,144} dobutamine,^{10,145–148} and dipyridamole,^{11,149} with high feasibility and good sensitivity and specificity for the detection of angiographic coronary artery disease. Three-dimensional stress echocardiography has also been successfully combined with contrast.^{150,151} Although a learning curve is required to perform 3D stress echocardiography adequately, advantages of 3D stress echocardiography include (1) better visualization of the LV apex, which is frequently foreshortened on standard 2DE apical images; (2) rapid acquisition of peak stress images before the heart rate declines in recovery; and (3) evaluation of multiple segments from different planes from a single data set. Disadvantages include lower spatial resolution and lower frame rates. Moreover, only recently has 3DE technology allowed side-by-side display of rest and stress images for comparison.¹¹

a. Acquisition Methods

Matrix-array transducers allow different approaches to perform multiplanar or 3D stress echocardiography. Whether two or even three image planes can be recorded simultaneously depends on the capabilities of the equipment.

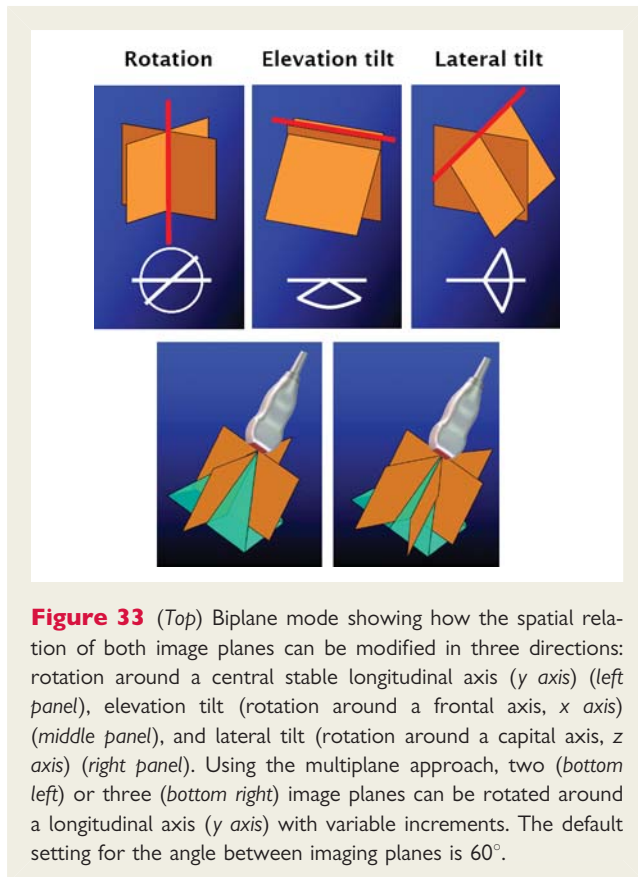


Figure 33 (Top) Biplane mode showing how the spatial relation of both image planes can be modified in three directions: rotation around a central stable longitudinal axis (y axis) (left panel), elevation tilt (rotation around a frontal axis, x axis) (middle panel), and lateral tilt (rotation around a capital axis, z axis) (right panel). Using the multiplane approach, two (bottom left) or three (bottom right) image planes can be rotated around a longitudinal axis (y axis) with variable increments. The default setting for the angle between imaging planes is 60° .

In biplane mode, the spatial relation of both image planes can be modified in three directions: rotation around a central stable longitudinal axis, elevation, and lateral tilt (Figure 33). Using the triplane approach, three image planes can be rotated around a longitudinal axis (the y axis) with variable increments (Figure 9). The spatial and temporal resolution of the images acquired with a matrix array transducer in biplane and triplane scanning modes are similar to conventional 2D images. However, the acquisition time is shorter because two or three planes are simultaneously captured.

The acquisition of gated 3DE data sets allows analysis of the complete circumference of the LV wall and not only two or three selected image planes with the corresponding wall segments, which can lead to image plane positioning errors. Temporal resolution depends on the number of acquired subvolumes and segment depth but regularly lies between 30 and 50 volumes/sec. The smaller the number or the wider the angle of the acquired subsegments, the lower spatial and time resolution will be. Single-beat acquisition of full-volume LV data is a recent development from some vendors, and the spatial and temporal resolution of these systems are currently being evaluated.

b. Data Acquisition

Like conventional 2D techniques, 3D echocardiography during stress can be performed at rest, at low and peak load or dose, and during recovery. Both physical stress (either bicycle or treadmill exercise) and pharmacologic stress (mainly dobutamine plus

atropine) can be used in combination with 3D echocardiography. The use of dipyridamole offers the advantage of not increasing the heart rate significantly, which is of value when using a technique that has limited temporal resolution. Left-heart contrast agents can be used for improved endocardial delineation as continuous infusion or bolus injections immediately before the acquisition of images at each stress level. However, for gated 3DE data sets acquired over several cardiac cycles, contrast infusions are preferred to maintain a constant concentration of microbubbles during data acquisition. Many 3DE systems currently have contrast specific settings, similar to those used with 2D echocardiography.

Biplane Mode

This mode allows the simultaneous acquisition of the parasternal long axis and an adapted parasternal short axis, which can be best achieved by laterally tilting the second plane 30° to 40° in the apical direction. From the apical approach, acquisition using a biplane mode starts with simultaneous apical four-chamber and two-chamber views. The orientation of the matrix transducer is first optimized to obtain an anatomically correct four-chamber view on the left image screen. Using the rotation around the stable y axis (longitudinal rotation), the second image plane (i.e., right screen) is turned to about 30° so that the inferior wall is seen on the left and the anterior segments on the right image side. Then, the right image is rotated to about 240° , resulting in an apical long axis with the posterior wall to the left and the antero-septal segments to the right. The other biplane image (i.e., left screen) remains stable, showing the apical four-chamber-view. Thus, three heartbeats must be acquired serially from two echocardiographic windows to record all necessary image planes. Image plane orientation must be stored in the echocardiographic equipment as individual settings to enable side-by-side visualization for comparison of rest and stress images.

Triplane Mode

Acquisition of triplane data is typically not performed from the parasternal window but rather from a single apical echocardiographic window. In most patients, a default setting of 60° increments between the three planes allows the simultaneous visualization of the four-chamber and two-chamber views as well as the apical long axis. Furthermore, when omitting parasternal recordings, triplane scanning facilitates a single transducer position for the acquisition of images at each stress stage. Loops from all three image planes are stored separately and analyzed side by side in a manner comparable with that of conventional 2D stress echocardiography.

Gated Mode

The acquisition of gated 3DE data sets during stress further decreases the number of serially acquired heartbeats. Stress echocardiographic acquisition of full-volume data is normally performed from a single apical approach, similar to that of the triplane modality. Parasternal gated 3DE recordings in the majority of patients are not able to encompass the entire left ventricle and therefore are not recommended. A minimum of a single full-volume data set should be acquired at each stress level. The main difference

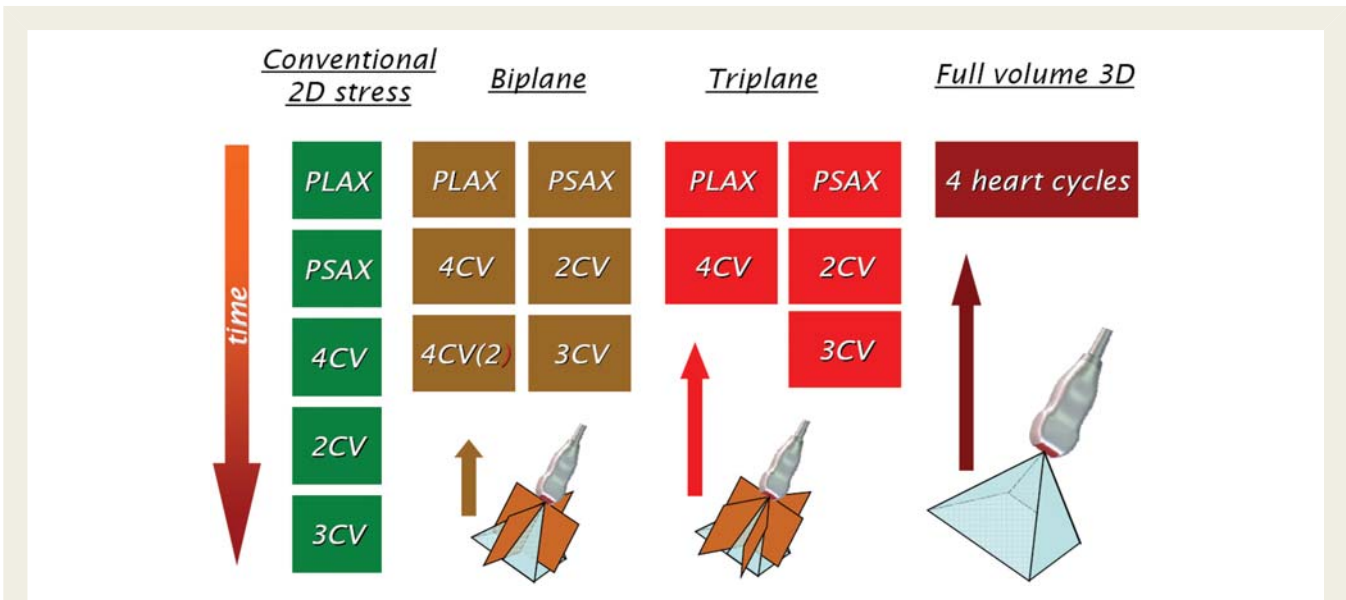


Figure 34 Diagram illustrating the differences between conventional 2DE, multiplanar, and full-volume 3D imaging modes in the number of separate views that must be acquired for a complete echocardiographic stress study. As the number of acquisitions decreases, the scanning time required to complete the study becomes shorter. 4CV, Four-chamber view; PLAX, parasternal long-axis; PSAX, parasternal short-axis; 3CV, three-chamber view; 2CV, two-chamber view.

between conventional 2DE and multiplanar and especially full-volume 3D stress echocardiography is the significantly shorter scanning time required to complete the study.

On the basis of this rapid method of data acquisition, the narrow time window at peak stress, especially during physical exercise echocardiography, can be used more effectively when acquiring a complete 3DE data set. Performing stress echo in a biplane or triplane approach results in a higher heart rate during exercise stress acquisition, thus facilitating ischemia detection. Furthermore, there is no need to change the transducer position during apical scanning once the optimal window is identified. This makes acquisition easier and faster for both beginner and expert echocardiographers (Figure 34).

c. Analysis Methods

A 3DE full-volume data set incorporating the entire left ventricle is required for analysis. To optimize the volume rate, the size of the data set should be adjusted during acquisition so that extraneous structures such as the right ventricle and left atrium are excluded. Furthermore, if the 3D ultrasound system has an option for increasing volume rates (perhaps by using more subvolumes), that option should be selected.

On some 3DE systems, single-beat full-volume acquisitions can be performed at reasonable volume rates, thereby avoiding subvolume stitch artifacts. Indeed, if the data set has been created using subvolumes, it is important to validate its integrity before proceeding with the analysis. This is achieved by cropping down from the apex in a transverse plane, inspecting for stitching artifacts between subvolumes. For analysis, a full-volume data set of the left ventricle can be cropped in a number of different ways using slicing techniques to create semiconventional 2D “slices” of the left ventricle (Figure 4). These would typically include the three longitudinal

planes: apical four-chamber, two-chamber, long-axis, and a series of transverse (short-axis) planes. The latter planes are usually six or nine in number and are conventionally arranged in equidistant intervals from the base of the left ventricle to the apex (Figure 35). This is analogous to the display methodology used in magnetic resonance imaging.

An important advantage of acquiring apical full-volume data sets that incorporate the entire left ventricle is the avoidance of foreshortening. Although higher image quality on apical 2D echocardiography can often be obtained by using a higher intercostal space, this results in foreshortening of the left ventricle so that the true LV apex is not visualized. This can be avoided using 3D echocardiography because, if the entire left ventricle is incorporated within the data set, postacquisition cropping can be used to create 2DE equivalent images that are not foreshortened. Furthermore, the use of slicing with adjustment of the planes in three vectors facilitates geometric correction and ensures that no plane is off axis. With 3D, every plane can be adjusted to ensure that it is correct geometrically and that it correlates with other planes acquired at different stress stages.

However, manual cropping of the LV data set is time consuming. Therefore, 3D stress echocardiographic software incorporating auto-cropping features that create standard 2D slices on the basis of the presumption that the apical full-volume data set has been acquired using a standard orientation. The auto-cropped planes could then be manually adjusted at baseline to achieve the desired views. This manual cropping adjustment could be used as a template, which the software will then use to create views at subsequent stress stages. Again, manual adjustments should be possible at each stage. Some 3D stress software uses feature extraction techniques that incorporate preloaded 3D image templates. Pattern recognition is used to identify anatomic

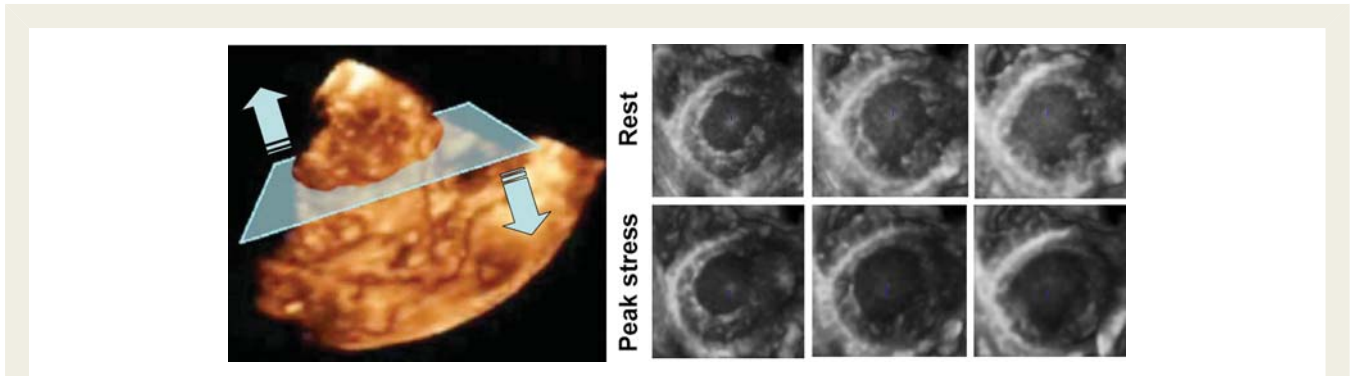


Figure 35 A 3D TTE full volume data set can be acquired from the apical window (left) and later cropped into a number of transverse slices from the apex to the base of the left ventricle (right). This imaging display is especially useful during 3D stress studies.

landmarks within the 3D data set, simplifying and allowing an automated cropping process. In addition to the use of the slicing technique that creates “standard” 2D views from the 3D data set, it is also possible to continuously move or rotate the cropping plane during playback to effectively create an infinite number of planes. For example, a four-chamber equivalent plane could be slowly rotated through 180° to help identify off-axis wall motion abnormalities that might otherwise be missed.

d. Orientation and Display

Conventional 2D stress echocardiograms are usually analyzed by displaying the same view at different stages side by side. It would be therefore more familiar for most users if the multislice format derived from stress 3D data sets would also be displayed in a side-by-side format. New 3D stress software allows this feature, and it is recommended to use this display methodology when available. There is a limit to the number of views that can be simultaneously displayed on a monitor with appropriate size and resolution to facilitate analysis. An alternative display mode would be to select just one view and display it simultaneously with the same view obtained at other stages.

e. Clinical Validation and Application

Multislice views from 3DE stress studies should be interpreted in a similar way as conventional 2D stress studies evaluating stress-induced wall motion and thickening abnormalities. Side-by-side display of baseline and the various stress-stage images facilitates this. Adjustment of the image planes to avoid foreshortening and ensure reproducibility of the scan planes between stages will further increase the accuracy of 3DE stress techniques. In evaluating the diagnostic and prognostic value of stress echocardiography, it has been demonstrated that it is not only the presence and severity of stress-induced regional wall motion abnormalities that are related to the extent of coronary disease and predictive of outcome, but changes in ejection fraction and ventricular volume have been also shown to be equally important.^{152,153} By permitting more accurate assessment of LV volume and ejection fraction, especially in patients with resting

wall motion abnormalities, 3D echocardiography has a potential to further improve the accuracy of 2D stress echocardiography but is still limited by temporal resolution.

LV dyssynchrony, which is analogous to tardokinesis, is also a marker for stress-induced ischemia and can be detected by 3D echocardiography as well as by other techniques. Three-dimensional stress studies using dynamic maps of contraction (Figure 11, lower left) may more accurately localize and estimate the severity of stress-induced ischemia by identifying areas of delayed contraction.

Because of its ability to acquire the entire LV volume within one beat, 3D stress transthoracic echocardiography holds promise for incorporation into clinical practice in the future.

18. Conclusions

Three-dimensional transthoracic echocardiography currently complements routine 2D echocardiography in daily clinical practice by providing additional volumetric information. However, its full complementary potential has not been exploited. Table 7 describes the opinions of the writing group on the basis of available literature regarding the utility of 3D echocardiography in the assessment of cardiac function and structures. This recommendation paper is aimed to be a practical technical operation document for 3D transthoracic echocardiography and transesophageal echocardiography with current standard echocardiographic systems and on-cart software. The details will become obsolete with future systems and software, but once having started clinical 3D echocardiography with a full understanding of basic terminology and menus, one can more easily follow future evolution. However, it is important that 3D images be displayed in a uniform manner to facilitate interpretation and comparisons between studies (Table 5 and 6). In the near future, the ability to acquire a single-heartbeat full-volume data set with higher temporal and spatial resolution, and live 3DE color Doppler imaging with a larger angle, should be feasible. All these will continue to enhance 3DE utility and efficiency in daily clinical practice.

Table 7 Summary of indications for 3D echocardiography

	Recommended for Clinical Practice	Promising Clinical Studies	Areas of Active Research	Unstudied
Left Ventricle Functional Assessment				
Volume	✓			
Shape			✓	
Ejection Fraction	✓			
Dyssynchrony			✓	
Mass		✓		
Right Ventricle Functional Assessment				
Volume		✓		
Shape				✓
Ejection Fraction		✓		
Left Atrial Assessment				
Volume			✓	
Right Atrial Assessment				
Volume				✓
Mitral Valve Assessment				
Anatomy	✓			
Stenosis	✓			
Regurgitation			✓	
Tricuspid Valve Assessment				
Anatomy				✓
Stenosis				✓
Regurgitation				✓
Pulmonic Valve Assessment				
Anatomy				✓
Stenosis				✓
Regurgitation				✓
Aortic Valve Assessment				
Anatomy		✓		
Stenosis		✓		
Regurgitation				✓
Infective Endocarditis				
Prosthetic Valves			✓	✓
Guidance of Transcatheter Procedures*				
	✓			

*mitral clips, mitral valvuloplasty, transcatheter aortic valve Implantation, paravalvular leak closure, atrial septal defect closure, ventricular septal defect closure and left atrial appendage closure.

Notice and Disclaimer

This report is made available by the ASE and the EAE as a courtesy reference source for their members. This report contains recommendations only and should not be used as the sole basis to make medical practice decisions or for disciplinary action against any employee. The statements and recommendations contained in this report are based primarily on the opinions of experts, rather than on scientifically verified data. The ASE and EAE make no express or implied warranties regarding the completeness or accuracy of the information in this report, including the warranty of merchantability or fitness for a particular purpose. In no event shall the ASE or EAE be liable to you, your patients, or any other third parties for any decision made or action taken by you

or such other parties in reliance on this information. Nor does your use of this information constitute the offering of medical advice by the ASE or EAE or create any physician-patient relationship between the ASE, EAE, and your patients or anyone else.

References

1. Hung J, Lang R, Flachskampf F, Sherman SK, McCulloch ML, Adams DB et al. 3D echocardiography: a review of the current status and future directions. *J Am Soc Echocardiogr* **20** (2007) 213–233.
2. Fenster A, Downey DB, Cardinal HN. Three-dimensional ultrasound imaging. *Phys Med Biol* **46** (2001) R67–R99.
3. Cao QL, Pandian NG, Azevedo J, Schwartz SL, Vogel M, Fulton D et al. Enhanced comprehension of dynamic cardiovascular anatomy by three-dimensional echocardiography with the use of mixed shading techniques. *Echocardiography* **11** (1994) 627–633.

4. Rankin RN, Fenster A, Downey DB, Munk PL, Levin MF, Vellet AD. Three-dimensional sonographic reconstruction: techniques and diagnostic applications. *AJR Am J Roentgenol* **161** (1993) 695–702.
5. Pandian NG, Roelandt J, Nanda NC, Sugeng L, Cao QL, Azevedo J *et al*. Dynamic three-dimensional echocardiography: methods and clinical potential. *Echocardiography* **11** (1994) 237–259.
6. Yang HS, Bansal RC, Mookadam F, Khandheria BK, Tajik AJ, Chandrasekaran K. Practical guide for three-dimensional transthoracic echocardiography using a fully sampled matrix array transducer. *J Am Soc Echocardiogr* **21** (2008) 979–989.
7. Zamorano J, Cordeiro P, Sugeng L, Perez de Isla L, Weinert L, Macaya C *et al*. Real-time three-dimensional echocardiography for rheumatic mitral valve stenosis evaluation: an accurate and novel approach. *J Am Coll Cardiol* **43** (2004) 2091–2096.
8. Matsumura Y, Fukuda S, Tran H, Greenberg NL, Agler DA, Wada N *et al*. Geometry of the proximal isovelocity surface area in mitral regurgitation by 3-dimensional color Doppler echocardiography: difference between functional mitral regurgitation and prolapse regurgitation. *Am Heart J* **155** (2008) 231–238.
9. Cheng TO, Xie MX, Wang XF, Wang Y, Lu Q. Real-time 3-dimensional echocardiography in assessing atrial and ventricular septal defects: an echocardiographic-surgical correlative study. *Am Heart J* **148** (2004) 1091–1095.
10. Yoshitani H, Takeuchi M, Mor-Avi V, Otsuji Y, Hozumi T, Yoshizawa M. Comparative diagnostic accuracy of multiplane and multislice three-dimensional dobutamine stress echocardiography in the diagnosis of coronary artery disease. *J Am Soc Echocardiogr* **22** (2009) 437–442.
11. Badano LP, Muraru D, Rigo F, Del Mestre L, Ermacora D, Gianfagna P *et al*. High volume-rate three-dimensional stress echocardiography to assess inducible myocardial ischemia: a feasibility study. *J Am Soc Echocardiogr* **23** (2010) 628–635.
12. Mor-Avi V, Sugeng L, Lang RM. Real-time 3-dimensional echocardiography: an integral component of the routine echocardiographic examination in adult patients? *Circulation* **119** (2009) 314–329.
13. Kahlert P, Plicht B, Schenk IM, Janosi RA, Erbel R, Buck T. Direct assessment of size and shape of noncircular vena contracta area in functional versus organic mitral regurgitation using real-time three-dimensional echocardiography. *J Am Soc Echocardiogr* **21** (2008) 912–921.
14. Muraru D, Cardillo M, Livi U, Badano LP. 3-dimensional transesophageal echocardiographic assessment of papillary muscle rupture complicating acute myocardial infarction. *J Am Coll Cardiol* **56** (2010) e45.
15. Vegas A, Meineri M. Core review: three-dimensional transesophageal echocardiography is a major advance for intraoperative clinical management of patients undergoing cardiac surgery: a core review. *Anesth Analg* **110** (2010) 1548–1573.
16. Moustafa SE, Chandrasekaran K, Khandheria B, Tajik J, Mookadam F. Real-time three-dimensional transesophageal echocardiography assessment of the mitral valve: perioperative advantages and game-changing findings. *J Heart Valve Dis* **20** (2011) 114–122.
17. Faletra FF, Regoli F, Nucifora G, Auricchio A. Real-time, fluoroscopy, anatomic-guided catheter navigation by 3D TEE during ablation procedures. *JACC Cardiovasc Imaging* **4** (2011) 203–206.
18. Altiok E, Hamada S, van Hall S, Hanenberg M, Dohmen G, Almalla M *et al*. Comparison of direct planimetry of mitral valve regurgitation orifice area by three-dimensional transesophageal echocardiography to effective regurgitant orifice area obtained by proximal flow convergence method and vena contracta area determined by color Doppler echocardiography. *Am J Cardiol* **107** (2011) 452–458.
19. Biaggi P, Gruner C, Jedrziewicz S, Karski J, Meineri M, Vegas A *et al*. Assessment of mitral valve prolapse by 3D TEE angled views are key. *JACC Cardiovasc Imaging* **4** (2011) 94–97.
20. Otani K, Takeuchi M, Kaku K, Sugeng L, Yoshitani H, Haruki N *et al*. Assessment of the aortic root using real-time 3D transesophageal echocardiography. *Circ J* **74** (2010) 2649–2657.
21. Pushparajah K, Miller OI, Simpson JM. 3D echocardiography of the atrial septum: anatomical features and landmarks for the echocardiographer. *JACC Cardiovasc Imaging* **3** (2010) 981–984.
22. Faletra FF, Ho SY, Auricchio A. Anatomy of right atrial structures by real-time 3D transesophageal echocardiography. *JACC Cardiovasc Imaging* **3** (2010) 966–975.
23. Lee AP, Lam YY, Yip GW, Lang RM, Zhang Q, Yu CM. Role of real time three-dimensional transesophageal echocardiography in guidance of interventional procedures in cardiology. *Heart* **96** (2010) 1485–1493.
24. Flachskampf FA, Badano L, Daniel WG, Feneck RO, Fox KF, Fraser AG *et al*. Recommendations for transesophageal echocardiography: update 2010. *Eur J Echocardiogr* **11** (2010) 557–576.
25. Monaghan MJ. Role of real time 3D echocardiography in evaluating the left ventricle. *Heart* **92** (2006) 131–136.
26. Caiani EG, Coon P, Corsi C, Goonewardena S, Bardo D, Rafter P *et al*. Dual triggering improves the accuracy of left ventricular volume measurements by contrast-enhanced real-time 3-dimensional echocardiography. *J Am Soc Echocardiogr* **18** (2005) 1292–1298.
27. Nucifora G, Marsan NA, Holman ER, Siebelink HM, van Werkhoven JM, Scholte AJ *et al*. Real-time 3-dimensional echocardiography early after acute myocardial infarction: incremental value of echo-contrast for assessment of left ventricular function. *Am Heart J* **157** (2009) 882–888.
28. Jenkins C, Moir S, Chan J, Rakhit D, Haluska B, Marwick TH. Left ventricular volume measurement with echocardiography: a comparison of left ventricular opacification, three-dimensional echocardiography, or both with magnetic resonance imaging. *Eur Heart J* **30** (2009) 98–106.
29. Krenning BJ, Kirschbaum SV, Soliman OI, Nemes A, van Geuns RJ, Vletter WB *et al*. Comparison of contrast agent-enhanced versus non-contrast agent-enhanced real-time three-dimensional echocardiography for analysis of left ventricular systolic function. *Am J Cardiol* **100** (2007) 1485–1489.
30. Lang RM, Bierig M, Devereux RB, Flachskampf FA, Foster E, Pellikka PA *et al*. Recommendations for chamber quantification: a report from the American Society of Echocardiography's Guidelines and Standards Committee and the Chamber Quantification Writing Group, developed in conjunction with the European Association of Echocardiography, a branch of the European Society of Cardiology. *J Am Soc Echocardiogr* **18** (2005) 1440–1463.
31. Muraru D, Badano LP, Piccoli G, Gianfagna P, Del Mestre L, Ermacora D *et al*. Validation of a novel automated border-detection algorithm for rapid and accurate quantification of left ventricular volumes based on three-dimensional echocardiography. *Eur J Echocardiogr* **11** (2010) 359–368.
32. Mor-Avi V, Jenkins C, Kuhl HP, Nesser HJ, Marwick TH, Franke A *et al*. Real-time 3-dimensional echocardiographic quantification of left ventricular volumes: multicenter study for validation with magnetic resonance imaging and investigation of sources of error. *JACC Cardiovasc Imaging* **1** (2008) 413–423.
33. Mannaerts HF, van der Heide JA, Kamp O, Stoel MG, Twisk J, Visser CA. Early identification of left ventricular remodeling after myocardial infarction, assessed by transthoracic 3D echocardiography. *Eur Heart J* **25** (2004) 680–687.
34. Caiani EG, Corsi C, Zamorano J, Sugeng L, MacEneaney P, Weinert L *et al*. Improved semiautomated quantification of left ventricular volumes and ejection fraction using 3-dimensional echocardiography with a full matrix-array transducer: comparison with magnetic resonance imaging. *J Am Soc Echocardiogr* **18** (2005) 779–788.
35. Jenkins C, Bricknell K, Hanekom L, Marwick TH. Reproducibility and accuracy of echocardiographic measurements of left ventricular parameters using real-time three-dimensional echocardiography. *J Am Coll Cardiol* **44** (2004) 878–886.
36. Jacobs LD, Salgo IS, Goonewardena S, Weinert L, Coon P, Bardo D *et al*. Rapid online quantification of left ventricular volume from real-time three-dimensional echocardiographic data. *Eur Heart J* **27** (2006) 460–468.
37. Shiota T, McCarthy PM, White RD, Qin JX, Greenberg NL, Flamm SD *et al*. Initial clinical experience of real-time three-dimensional echocardiography in patients with ischemic and idiopathic dilated cardiomyopathy. *Am J Cardiol* **84** (1999) 1068–1073.
38. Lee D, Fuisz AR, Fan PH, Hsu TL, Liu CP, Chiang HT. Real-time 3-dimensional echocardiographic evaluation of left ventricular volume: correlation with magnetic resonance imaging—a validation study. *J Am Soc Echocardiogr* **14** (2001) 1001–1009.
39. Chan J, Jenkins C, Khafagi F, Du L, Marwick T. What is the optimal clinical technique for measurement of left ventricular volume after myocardial infarction? A comparative study of 3-dimensional echocardiography, single photon emission computed tomography, and cardiac magnetic resonance imaging. *J Am Soc Echocardiogr* **19** (2006) 192–201.
40. Sugeng L, Mor-Avi V, Weinert L, Niel J, Ebner C, Steringer-Mascherbauer R *et al*. Quantitative assessment of left ventricular size and function: side-by-side comparison of real-time three-dimensional echocardiography and computed tomography with magnetic resonance reference. *Circulation* **114** (2006) 654–661.
41. Corsi C, Lang RM, Veronesi F, Weinert L, Caiani EG, MacEneaney P *et al*. Volumetric quantification of global and regional left ventricular function from real-time three-dimensional echocardiographic images. *Circulation* **112** (2005) 1161–1170.
42. Bicudo LS, Tsutsui JM, Shiozaki A, Rochitte CE, Arteaga E, Mady C *et al*. Value of real time three-dimensional echocardiography in patients with hypertrophic cardiomyopathy: comparison with two-dimensional echocardiography and magnetic resonance imaging. *Echocardiography* **25** (2008) 717–726.
43. Zeidan Z, Erbel R, Barkhausen J, Hunold P, Bartel T, Buck T. Analysis of global systolic and diastolic left ventricular performance using volume-time curves by real-time three-dimensional echocardiography. *J Am Soc Echocardiogr* **16** (2003) 29–37.
44. Kuhl HP, Schreckenber M, Rulands D, Katoh M, Schafer W, Schummers G *et al*. High-resolution transthoracic real-time three-dimensional echocardiography:

- quantitation of cardiac volumes and function using semi-automatic border detection and comparison with cardiac magnetic resonance imaging. *J Am Coll Cardiol* **43** (2004) 2083–2090.
45. Gutierrez-Chico JL, Zamorano JL, Perez de Isla L, Orejas M, Almeria C, Rodrigo JL et al. Comparison of left ventricular volumes and ejection fractions measured by three-dimensional echocardiography versus by two-dimensional echocardiography and cardiac magnetic resonance in patients with various cardiomyopathies. *Am J Cardiol* **95** (2005) 809–813.
 46. Nikitin NP, Constantin C, Loh PH, Ghosh J, Lukaschuk EI, Bennett A et al. New generation 3-dimensional echocardiography for left ventricular volumetric and functional measurements: comparison with cardiac magnetic resonance. *Eur J Echocardiogr* **7** (2006) 365–372.
 47. van den Bosch AE, Robbers-Visser D, Krenning BJ, Voormolen MM, McGhie JS, Helbing WA et al. Real-time transthoracic three-dimensional echocardiographic assessment of left ventricular volume and ejection fraction in congenital heart disease. *J Am Soc Echocardiogr* **19** (2006) 1–6.
 48. Pouleur AC, le Polain de Waroux JB, Pasquet A, Gerber BL, Gerard O, Allain P et al. Assessment of left ventricular mass and volumes by three-dimensional echocardiography in patients with or without wall motion abnormalities: comparison against cine magnetic resonance imaging. *Heart* **94** (2008) 1050–1057.
 49. Qi X, Cogar B, Hsiung MC, Nanda NC, Miller AP, Yelamanchili P et al. Live/real time three-dimensional transthoracic echocardiographic assessment of left ventricular volumes, ejection fraction, and mass compared with magnetic resonance imaging. *Echocardiography* **24** (2007) 166–173.
 50. Soliman OI, Kirschbaum SW, van Dalen BM, van der Zwaan HB, Mahdavian DB, Vletter WB et al. Accuracy and reproducibility of quantitation of left ventricular function by real-time three-dimensional echocardiography versus cardiac magnetic resonance. *Am J Cardiol* **102** (2008) 778–783.
 51. Jenkins C, Chan J, Hanekom L, Marwick TH. Accuracy and feasibility of online 3-dimensional echocardiography for measurement of left ventricular parameters. *J Am Soc Echocardiogr* **19** (2006) 1119–1128.
 52. Shimada YJ, Shiota T. A meta-analysis investigation for the source of bias of left ventricular volumes function by three-dimensional echocardiography in comparison with magnetic resonance imaging. *Am J Cardiol* **107** (2011) 126–138.
 53. Caiani EG, Corsi C, Sugeng L, MacEneaney P, Weinert L, Mor-Avi V et al. Improved quantification of left ventricular mass based on endocardial and epicardial surface detection with real time three dimensional echocardiography. *Heart* **92** (2006) 213–219.
 54. Mor-Avi V, Sugeng L, Weinert L, MacEneaney P, Caiani EG, Koch R et al. Fast measurement of left ventricular mass with real-time three-dimensional echocardiography: comparison with magnetic resonance imaging. *Circulation* **110** (2004) 1814–1818.
 55. Qin JX, Jones M, Travaglini A, Song JM, Li J, White RD et al. The accuracy of left ventricular mass determined by real-time three-dimensional echocardiography in chronic animal and clinical studies: a comparison with postmortem examination and magnetic resonance imaging. *J Am Soc Echocardiogr* **18** (2005) 1037–1043.
 56. Oe H, Hozumi T, Arai K, Matsumura Y, Negishi K, Sugioka K et al. Comparison of accurate measurement of left ventricular mass in patients with hypertrophied hearts by real-time three-dimensional echocardiography versus magnetic resonance imaging. *Am J Cardiol* **95** (2005) 1263–1267.
 57. van den Bosch AE, Robbers-Visser D, Krenning BJ, McGhie JS, Helbing WA, Meijboom FJ et al. Comparison of real-time three-dimensional echocardiography to magnetic resonance imaging for assessment of left ventricular mass. *Am J Cardiol* **97** (2006) 113–117.
 58. Takeuchi M, Nishikage T, Mor-Avi V, Sugeng L, Weinert L, Nakai H et al. Measurement of left ventricular mass by real-time three-dimensional echocardiography: validation against magnetic resonance and comparison with two-dimensional and m-mode measurements. *J Am Soc Echocardiogr* **21** (2008) 1001–1005.
 59. Takeuchi M, Jacobs A, Sugeng L, Nishikage T, Nakai H, Weinert L et al. Assessment of left ventricular dyssynchrony with real-time 3-dimensional echocardiography: comparison with Doppler tissue imaging. *J Am Soc Echocardiogr* **20** (2007) 1321–1329.
 60. Marsan NA, Bleeker GB, Ypenburg C, Ghio S, van de Veire NR, Holman ER et al. Real-time three-dimensional echocardiography permits quantification of left ventricular mechanical dyssynchrony and predicts acute response to cardiac resynchronization therapy. *J Cardiovasc Electrophysiol* **19** (2008) 392–399.
 61. Marsan NA, Bleeker GB, Ypenburg C, van Bommel RJ, Ghio S, van de Veire NR et al. Real-time three-dimensional echocardiography as a novel approach to assess left ventricular and left atrium reverse remodeling and to predict response to cardiac resynchronization therapy. *Heart Rhythm* **5** (2008) 1257–1264.
 62. Kleijn SA, van Dijk J, de Cock CC, Allaart CP, van Rossum AC, Kamp O. Assessment of intraventricular mechanical dyssynchrony and prediction of response to cardiac resynchronization therapy: comparison between tissue Doppler imaging and real-time three-dimensional echocardiography. *J Am Soc Echocardiogr* **22** (2009) 1047–1054.
 63. Soliman OI, Geleijnse ML, Theuns DA, van Dalen BM, Vletter WB, Jordaens LJ et al. Usefulness of left ventricular systolic dyssynchrony by real-time three-dimensional echocardiography to predict long-term response to cardiac resynchronization therapy. *Am J Cardiol* **103** (2009) 1586–1591.
 64. Becker M, Hoffmann R, Schmitz F, Hundemer A, Kuhl H, Schauer P et al. Relation of optimal lead positioning as defined by three-dimensional echocardiography to long-term benefit of cardiac resynchronization. *Am J Cardiol* **100** (2007) 1671–1676.
 65. Mor-Avi V, Lang RM. The use of real-time three-dimensional echocardiography for the quantification of left ventricular volumes and function. *Curr Opin Cardiol* **24** (2009) 402–409.
 66. Monaghan M. Echocardiographic assessment of left ventricular dyssynchrony—is three-dimensional echocardiography just the latest kid on the block? *J Am Soc Echocardiogr* **22** (2009) 240–241.
 67. Perez de Isla L, Balcones DV, Fernandez-Golfín C, Marcos-Alberca P, Almeria C, Rodrigo JL et al. Three-dimensional-wall motion tracking: a new and faster tool for myocardial strain assessment: comparison with two-dimensional-wall motion tracking. *J Am Soc Echocardiogr* **22** (2009) 325–330.
 68. Mertens LL, Friedberg M.K. Imaging the right ventricle—current state of the art. *Nat Rev Cardiol* **7** (2010) 551–563.
 69. Mangion JR. Right ventricular imaging by two-dimensional and three-dimensional echocardiography. *Curr Opin Cardiol* **25** (2010) 423–429.
 70. Sukmawan R, Watanabe N, Ogasawara Y, Yamaura Y, Yamamoto K, Wada N et al. Geometric changes of tricuspid valve tenting in tricuspid regurgitation secondary to pulmonary hypertension quantified by novel system with transthoracic real-time 3-dimensional echocardiography. *J Am Soc Echocardiogr* **20** (2007) 470–476.
 71. Sugeng L, Mor-Avi V, Weinert L, Niel J, Ebner C, Steringer-Mascherbauer R et al. Multimodality comparison of quantitative volumetric analysis of the right ventricle. *JACC Cardiovasc Imaging* **3** (2010) 10–18.
 72. Shiota T. 3D echocardiography: evaluation of the right ventricle. *Curr Opin Cardiol* **24** (2009) 410–414.
 73. Tamborini G, Brusoni D, Torres Molina JE, Galli CA, Maltagliati A, Muratori M et al. Feasibility of a new generation three-dimensional echocardiography for right ventricular volumetric and functional measurements. *Am J Cardiol* **102** (2008) 499–505.
 74. Gopal AS, Chukwu EO, Iwuchukwu CJ, Katz AS, Toole RS, Schapiro W et al. Normal values of right ventricular size and function by real-time 3-dimensional echocardiography: comparison with cardiac magnetic resonance imaging. *J Am Soc Echocardiogr* **20** (2007) 445–455.
 75. Niemann PS, Pinho L, Balbach T, Galuschky C, Blankenhagen M, Silberbach M et al. Anatomically oriented right ventricular volume measurements with dynamic three-dimensional echocardiography validated by 3-Tesla magnetic resonance imaging. *J Am Coll Cardiol* **50** (2007) 1668–1676.
 76. Kjaergaard J, Petersen CL, Kjaer A, Schaadt BK, Oh JK, Hassager C. Evaluation of right ventricular volume and function by 2D and 3D echocardiography compared to MRI. *Eur J Echocardiogr* **7** (2006) 430–438.
 77. Kjaergaard J, Sogaard P, Hassager C. Quantitative echocardiographic analysis of the right ventricle in healthy individuals. *J Am Soc Echocardiogr* **19** (2006) 1365–1372.
 78. Tamborini G, Marsan NA, Gripari P, Maffessanti F, Brusoni D, Muratori M et al. Reference values for right ventricular volumes and ejection fraction with real-time three-dimensional echocardiography: evaluation in a large series of normal subjects. *J Am Soc Echocardiogr* **23** (2010) 109–115.
 79. Kjaergaard J, Hastrup SJ, Sogaard P, Chen X, Bay NH, Kober L et al. Advanced quantitative echocardiography in arrhythmogenic right ventricular cardiomyopathy. *J Am Soc Echocardiogr* **20** (2007) 27–35.
 80. Acar P, Abadir S, Roux D, Taktak A, Dulac Y, Glock Y et al. Ebstein's anomaly assessed by real-time 3-D echocardiography. *Ann Thorac Surg* **82** (2006) 731–733.
 81. Grewal J, Majdalany D, Syed I, Pellikka P, Warnes CA. Three-dimensional echocardiographic assessment of right ventricular volume and function in adult patients with congenital heart disease: comparison with magnetic resonance imaging. *J Am Soc Echocardiogr* **23** (2010) 127–133.
 82. Scheurer M, Bandisodé V, Ruff P, Atz A, Shirali G. Early experience with real-time three-dimensional echocardiographic guidance of right ventricular biopsy in children. *Echocardiography* **23** (2006) 45–49.
 83. Tamborini G, Muratori M, Brusoni D, Celeste F, Maffessanti F, Caiani EG et al. Is right ventricular systolic function reduced after cardiac surgery? A two- and three-dimensional echocardiographic study. *Eur J Echocardiogr* **10** (2009) 630–634.

84. Lancellotti P, Moura L, Pierard LA, Agricola E, Popescu BA, Tribouilloy C *et al*. European Association of Echocardiography recommendations for the assessment of valvular regurgitation. Part 2: mitral and tricuspid regurgitation (native valve disease). *Eur J Echocardiogr* **11** (2010) 307–332.
85. Levine RA, Durst R. Mitral valve prolapse: a deeper look. *JACC Cardiovasc Imaging* **1** (2008) 304–306.
86. Sugeng L, Coon P, Weinert L, Jolly N, Lammertin G, Bednarz JE *et al*. Use of real-time 3-dimensional transthoracic echocardiography in the evaluation of mitral valve disease. *J Am Soc Echocardiogr* **19** (2006) 413–421.
87. Gutierrez-Chico JL, Zamorano Gomez JL, Rodrigo-Lopez JL, Mataix L, Perez de Isla L, Almeria-Valera C *et al*. Accuracy of real-time 3-dimensional echocardiography in the assessment of mitral prolapse. Is transesophageal echocardiography still mandatory? *Am Heart J* **155** (2008) 694–698.
88. Tamborini G, Muratori M, Maltagliati A, Galli CA, Naliato M, Zanobini M *et al*. Pre-operative transthoracic real-time three-dimensional echocardiography in patients undergoing mitral valve repair: accuracy in cases with simple vs. complex prolapse lesions. *Eur J Echocardiogr* **11** (2010) 778–785.
89. Pepi M, Tamborini G, Maltagliati A, Galli CA, Sisillo E, Salvi L *et al*. Head-to-head comparison of two- and three-dimensional transthoracic and transesophageal echocardiography in the localization of mitral valve prolapse. *J Am Coll Cardiol* **48** (2006) 2524–2530.
90. Grewal J, Mankad S, Freeman WK, Click RL, Suri RM, Abel MD *et al*. Real-time three-dimensional transesophageal echocardiography in the intraoperative assessment of mitral valve disease. *J Am Soc Echocardiogr* **22** (2009) 34–41.
91. Garcia-Fernandez MA, Cortes M, Garcia-Robles JA, Gomez de Diego JJ, Perez-David E, Garcia E. Utility of real-time three-dimensional transesophageal echocardiography in evaluating the success of percutaneous transcatheter closure of mitral paravalvular leaks. *J Am Soc Echocardiogr* **23** (2010) 26–32.
92. Becerra JM, Almeria C, Perez de Isla L, Zamorano J. Usefulness of 3D transesophageal echocardiography for guiding wires and closure devices in mitral paravalvular leaks. *Eur J Echocardiogr* **10** (2009) 979–981.
93. Kim MS, Casserly IP, Garcia JA, Klein AJ, Salcedo EE, Carroll JD. Percutaneous transcatheter closure of prosthetic mitral paravalvular leaks: are we there yet? *JACC Cardiovasc Interv* **2** (2009) 81–90.
94. Tsang W, Lang RM, Kronzon I. Role of real-time three dimensional echocardiography in cardiovascular interventions. *Heart* **97** (2011) 850–857.
95. Chandra S, Salgo IS, Sugeng L, Weinert L, Settlemier SH, Mor-Avi V *et al*. A three-dimensional insight into the complexity of flow convergence in mitral regurgitation: adjunctive benefit of anatomic regurgitant orifice area. *Am J Physiol Heart Circ Physiol* **301** (2011) H1015–H1024.
96. Perez de Isla L, Casanova C, Almeria C, Rodrigo JL, Cordeiro P, Mataix L *et al*. Which method should be the reference method to evaluate the severity of rheumatic mitral stenosis? Gorlin's method versus 3D-echo. *Eur J Echocardiogr* **8** (2007) 470–473.
97. Anwar AM, Attia WM, Nosir YF, Soliman OI, Mosad MA, Othman M *et al*. Validation of a new score for the assessment of mitral stenosis using real-time three-dimensional echocardiography. *J Am Soc Echocardiogr* **23** (2010) 13–22.
98. De SR, Glombitza G, Vahl CF, Albers J, Meinzer HP, Hagl S. Three-dimensional color Doppler: a clinical study in patients with mitral regurgitation. *J Am Coll Cardiol* **33** (1999) 1646–1654.
99. Anderson RH. Clinical anatomy of the aortic root. *Heart* **84** (2000) 670–673.
100. Kasprzak JD, Nosir YF, Dall'Agata A, Elhendy A, Taams M, Ten Cate FJ *et al*. Quantification of the aortic valve area in three-dimensional echocardiographic data sets: analysis of orifice overestimation resulting from suboptimal cut-plane selection. *Am Heart J* **135** (1998) 995–1003.
101. Suradi H, Byers S, Green-Hess D, Gradus-Pizlo I, Sawada S, Feigenbaum H. Feasibility of using real time "live 3D" echocardiography to visualize the stenotic aortic valve. *Echocardiography* **27** (2010) 1011–1020.
102. de la Morena G, Saura D, Oliva MJ, Soria F, Gonzalez J, Garcia M *et al*. Real-time three-dimensional transesophageal echocardiography in the assessment of aortic valve stenosis. *Eur J Echocardiogr* **11** (2010) 9–13.
103. Nakai H, Takeuchi M, Yoshitani H, Kaku K, Haruki N, Otsuji Y. Pitfalls of anatomical aortic valve area measurements using two-dimensional transesophageal echocardiography and the potential of three-dimensional transesophageal echocardiography. *Eur J Echocardiogr* **11** (2010) 369–376.
104. Gutierrez-Chico JL, Zamorano JL, Prieto-Moriche E, Hernandez-Antolin RA, Bravo-Amaro M, Perez de Isla L *et al*. Real-time three-dimensional echocardiography in aortic stenosis: a novel, simple, and reliable method to improve accuracy in area calculation. *Eur Heart J* **29** (2008) 1296–1306.
105. Poh KK, Levine RA, Solis J, Shen L, Flaherty M, Kang YJ *et al*. Assessing aortic valve area in aortic stenosis by continuity equation: a novel approach using real-time three-dimensional echocardiography. *Eur Heart J* **29** (2008) 2526–2535.
106. Goland S, Trento A, Iida K, Czer LS, De RM, Naqvi TZ *et al*. Assessment of aortic stenosis by three-dimensional echocardiography: an accurate and novel approach. *Heart* **93** (2007) 801–807.
107. Ge S, Warner J.G Jr, Abraham TP, Kon ND, Brooker RF, Nomeir AM *et al*. Three-dimensional surface area of the aortic valve orifice by three-dimensional echocardiography: clinical validation of a novel index for assessment of aortic stenosis. *Am Heart J* **136** (1998) 1042–1050.
108. Messika-Zeitoun D, Serfaty JM, Brochet E, Ducrocq G, Lepage L, Detaint D *et al*. Multimodal assessment of the aortic annulus diameter: implications for transcatheter aortic valve implantation. *J Am Coll Cardiol* **55** (2010) 186–194.
109. Doddamani S, Bello R, Friedman MA, Banerjee A, Bowers J.H Jr, Kim B *et al*. Demonstration of left ventricular outflow tract eccentricity by real time 3D echocardiography: implications for the determination of aortic valve area. *Echocardiography* **24** (2007) 860–866.
110. Shahgaldi K, Manouras A, Brodin LA, Winter R. Direct measurement of left ventricular outflow tract area using three-dimensional echocardiography in biplane mode improves accuracy of stroke volume assessment. *Echocardiography* **27** (2010) 1078–1085.
111. Doddamani S, Grushko MJ, Makaryus AN, Jain VR, Bello R, Friedman MA *et al*. Demonstration of left ventricular outflow tract eccentricity by 64-slice multi-detector CT. *Int J Cardiovasc Imaging* **25** (2009) 175–181.
112. Chin CH, Chen CH, Lo H.S. The correlation between three-dimensional vena contracta area and aortic regurgitation index in patients with aortic regurgitation. *Echocardiography* **27** (2010) 161–166.
113. Fang L, Hsiung MC, Miller AP, Nanda NC, Yin WH, Young MS *et al*. Assessment of aortic regurgitation by live three-dimensional transthoracic echocardiographic measurements of vena contracta area: usefulness and validation. *Echocardiography* **22** (2005) 775–781.
114. Kelly NF, Platts DG, Burstow DJ. Feasibility of pulmonary valve imaging using three-dimensional transthoracic echocardiography. *J Am Soc Echocardiogr* **23** (2010) 1076–1080.
115. Anwar AM, Soliman O, van den Bosch AE, McGhie JS, Geleijnse ML, Ten Cate FJ *et al*. Assessment of pulmonary valve and right ventricular outflow tract with real-time three-dimensional echocardiography. *Int J Cardiovasc Imaging* **23** (2007) 167–175.
116. Pothineni KR, Wells BJ, Hsiung MC, Nanda NC, Yelamanchili P, Suwanjutha T *et al*. Live/real time three-dimensional transthoracic echocardiographic assessment of pulmonary regurgitation. *Echocardiography* **25** (2008) 911–917.
117. Fukuda S, Saracino G, Matsumura Y, Daimon M, Tran H, Greenberg NL *et al*. Three-dimensional geometry of the tricuspid annulus in healthy subjects and in patients with functional tricuspid regurgitation: a real-time, 3-dimensional echocardiographic study. *Circulation* **114** (2006) 1492–1498.
118. Ton-Nu TT, Levine RA, Handschumacher MD, Dorer DJ, Yosefy C, Fan D *et al*. Geometric determinants of functional tricuspid regurgitation: insights from 3-dimensional echocardiography. *Circulation* **114** (2006) 143–149.
119. Anwar AM, Soliman OI, Nemes A, van Geuns RJ, Geleijnse ML, Ten Cate FJ. Value of assessment of tricuspid annulus: real-time three-dimensional echocardiography and magnetic resonance imaging. *Int J Cardiovasc Imaging* **23** (2007) 701–705.
120. Anwar AM, Geleijnse ML, Soliman OI, McGhie JS, Frowijn R, Nemes A *et al*. Assessment of normal tricuspid valve anatomy in adults by real-time three-dimensional echocardiography. *Int J Cardiovasc Imaging* **23** (2007) 717–724.
121. Muraru D, Badano LP, Sarais C, Solda E, Illiceto S. Evaluation of tricuspid valve morphology and function by transthoracic three-dimensional echocardiography. *Curr Cardiol Rep* **13** (2011) 242–249.
122. Badano LP, Agricola E, Perez de Isla L, Gianfagna P, Zamorano JL. Evaluation of the tricuspid valve morphology and function by transthoracic real-time three-dimensional echocardiography. *Eur J Echocardiogr* **10** (2009) 477–484.
123. Pothineni KR, Duncan K, Yelamanchili P, Nanda NC, Patel V, Fan P *et al*. Live/real time three-dimensional transthoracic echocardiographic assessment of tricuspid valve pathology: incremental value over the two-dimensional technique. *Echocardiography* **24** (2007) 541–552.
124. Abadir S, Leobon B, Acar P. Assessment of tricuspid regurgitation mechanism by three-dimensional echocardiography in an adult patient with congenitally corrected transposition of the great arteries. *Arch Cardiovasc Dis* **102** (2009) 459–460.
125. Enar S, Singh P, Douglas C, Panwar SR, Manda J, Kesanolla SK *et al*. Live/real time three-dimensional transthoracic echocardiographic assessment of transposition of the great arteries in the adult. *Echocardiography* **26** (2009) 1095–1104.
126. Takahashi K, Inage A, Rebeyka IM, Ross DB, Thompson RB, Mackie AS *et al*. Real-time 3-dimensional echocardiography provides new insight into mechanisms of tricuspid valve regurgitation in patients with hypoplastic left heart syndrome. *Circulation* **120** (2009) 1091–1098.
127. Seo Y, Ishizu T, Nakajima H, Sekiguchi Y, Watanabe S, Aonuma K. Clinical utility of 3-dimensional echocardiography in the evaluation of tricuspid regurgitation caused by pacemaker leads. *Circ J* **72** (2008) 1465–1470.
128. Velayudhan DE, Brown TM, Nanda NC, Patel V, Miller AP, Mehmood F *et al*. Quantification of tricuspid regurgitation by live three-dimensional transthoracic

- echocardiographic measurements of vena contracta area. *Echocardiography* **23** (2006) 793–800.
129. Faletra FF, Nucifora G, Ho SY. Imaging the atrial septum using real-time three-dimensional transesophageal echocardiography: technical tips normal anatomy its role in transseptal puncture. *J Am Soc Echocardiogr* **24** (2011) 593–599.
 130. Loukas M, Tubbs RS, Tongson JM, Polepalli S, Curry B, Jordan R et al. The clinical anatomy of the crista terminalis, pectinate muscles and the teniae sagittalis. *Ann Anat* **190** (2008) 81–87.
 131. Olgin JE, Kalman JM, Saxon LA, Lee RJ, Lesh MD. Mechanism of initiation of atrial flutter in humans: site of unidirectional block and direction of rotation. *J Am Coll Cardiol* **29** (1997) 376–384.
 132. Cabrera JA, Sanchez-Quintana D, Ho SY, Medina A, Anderson RH. The architecture of the atrial musculature between the orifice of the inferior caval vein and the tricuspid valve: the anatomy of the isthmus. *J Cardiovasc Electrophysiol* **9** (1998) 1186–1195.
 133. Ho SY. Pulmonary vein ablation in atrial fibrillation: does anatomy matter? *J Cardiovasc Electrophysiol* **14** (2003) 156–157.
 134. Miyasaka Y, Tsujimoto S, Maeba H, Yuasa F, Takehana K, Dote K et al. Left atrial volume by real-time three-dimensional echocardiography: validation by 64-slice multidetector computed tomography. *J Am Soc Echocardiogr* **24** (2011) 680–686.
 135. Marsan NA, Tops LF, Holman ER, van de Veire NR, Zeppenfeld K, Boersma E et al. Comparison of left atrial volumes and function by real-time three-dimensional echocardiography in patients having catheter ablation for atrial fibrillation with persistence of sinus rhythm versus recurrent atrial fibrillation three months later. *Am J Cardiol* **102** (2008) 847–853.
 136. Delgado V, Vidal B, Sitges M, Tamborero D, Mont L, Berrueto A et al. Fate of left atrial function as determined by real-time three-dimensional echocardiography study after radiofrequency catheter ablation for the treatment of atrial fibrillation. *Am J Cardiol* **101** (2008) 1285–1290.
 137. Maurice SM, Palmer AS, Miller AJ, Greene R. Lymphatic drainage of the heart in the laboratory rat. *Lymphology* **34** (2001) 145–148.
 138. Syed TM, Halperin JL. Left atrial appendage closure for stroke prevention in atrial fibrillation: state of the art and current challenges. *Nat Clin Pract Cardiovasc Med* **4** (2007) 428–435.
 139. Ernst G, Stollberger C, Abzieher F, Veit-Dirscherl W, Bonner E, Bibus B et al. Morphology of the left atrial appendage. *Anat Rec* **242** (1995) 553–561.
 140. Palmer AS, Miller AJ, Greene R. The lymphatic drainage of the left ventricle in the Yucatan minipig. *Lymphology* **31** (1998) 30–33.
 141. Al-Saady NM, Obel OA, Camm AJ. Left atrial appendage: structure, function, and role in thromboembolism. *Heart* **82** (1999) 547–554.
 142. Veinot JP, Harry PJ, Gentile F, Khandheria BK, Bailey KR, Eickholt JT et al. Anatomy of the normal left atrial appendage: a quantitative study of age-related changes in 500 autopsy hearts: implications for echocardiographic examination. *Circulation* **96** (1997) 3112–3115.
 143. Walimbe V, Garcia M, Lalude O, Thomas J, Shekhar R. Quantitative real-time 3-dimensional stress echocardiography: a preliminary investigation of feasibility and effectiveness. *J Am Soc Echocardiogr* **20** (2007) 13–22.
 144. Peteiro J, Pinon P, Perez R, Monserrat L, Perez D, Castro-Beiras A. Comparison of 2- and 3-dimensional exercise echocardiography for the detection of coronary artery disease. *J Am Soc Echocardiogr* **20** (2007) 959–967.
 145. Aggeli C, Giannopoulos G, Misovoulos P, Roussakis G, Christoforatu E, Kokkinakis C et al. Real-time three-dimensional dobutamine stress echocardiography for coronary artery disease diagnosis: validation with coronary angiography. *Heart* **93** (2007) 672–675.
 146. Matsumura Y, Hozumi T, Arai K, Sugijoka K, Ujino K, Takemoto Y et al. Non-invasive assessment of myocardial ischaemia using new real-time three-dimensional dobutamine stress echocardiography: comparison with conventional two-dimensional methods. *Eur Heart J* **26** (2005) 1625–1632.
 147. Eroglu E, D'hooge J, Herbots L et al. Comparison of real-time tri-plane and conventional 2D dobutamine stress echocardiography for the assessment of coronary artery disease. *Eur Heart J* **27** (2006) 1719–1724.
 148. Yang HS, Pellikka PA, McCully RB, Oh JK, Kuzkuzke JA, Khandheria BK et al. Role of biplane and biplane echocardiographically guided 3-dimensional echocardiography during dobutamine stress echocardiography. *J Am Soc Echocardiogr* **19** (2006) 1136–1143.
 149. Varnero S, Santagata P, Pratali L, Basso M, Gandolfo A, Bellotti P. Head to head comparison of 2D vs real time 3D dipyridamole stress echocardiography. *Cardiovasc Ultrasound* **6** (2008) 31.
 150. Pulerwitz T, Hirata K, Abe Y, Otsuka R, Herz S, Okajima K et al. Feasibility of using a real-time 3-dimensional technique for contrast dobutamine stress echocardiography. *J Am Soc Echocardiogr* **19** (2006) 540–545.
 151. Takeuchi M, Otani S, Weinert L, Spencer KT, Lang RM. Comparison of contrast-enhanced real-time live 3-dimensional dobutamine stress echocardiography with contrast 2-dimensional echocardiography for detecting stress-induced wall-motion abnormalities. *J Am Soc Echocardiogr* **19** (2006) 294–299.
 152. Chuah SC, Pellikka PA, Roger VL, McCully RB, Seward JB. Role of dobutamine stress echocardiography in predicting outcome in 860 patients with known or suspected coronary artery disease. *Circulation* **97** (1998) 1474–1480.
 153. Arruda AM, McCully RB, Oh JK, Mahoney DW, Seward JB, Pellikka PA. Prognostic value of exercise echocardiography in patients after coronary artery bypass surgery. *Am J Cardiol* **87** (2001) 1069–1073.